Journal of Ovarian Research

RESEARCH

Open Access

Ginsenoside Rg1 promotes the efficacy of human amnion-derived mesenchymal stem cells in alleviating chemotherapy-induced premature ovarian insufficiency in rats

Jiali Zeng[1†], Lanhua Wu[1†], Qianru Zeng[1], Caijiao Peng[1], Yubin Huang[1] and Li Ling[1*]

Abstract

Background Premature ovarian insufficiency (POI) can cause multiple sequelae in young women and is currently incurable. Mesenchymal stem cell (MSC)-based treatment of POI shows great promise. However, some limitations affect their efficacy in POI treatment, and exploration of methods to improve their efficacy is necessary. This study aimed to explore whether Rg1 can improve the efficacy of human amnion-derived MSC (hAD-MSC) transplantation in the treatment of rats with chemotherapy-induced POI.

Methods hAD-MSCs were isolated from human amnions. One hundred female SD rats were divided into control, POI, Rg1, hAD-MSCs and Rg1 + hAD-MSCs groups. POI rat models were first established by intraperitoneal injection of cisplatin, and then the rats in the hAD-MSCs and Rg1 + hAD-MSCs groups were injected with PKH26-labelled hAD-MSCs via tail veins, while the rats in the Rg1 and Rg1 + hAD-MSCs groups were intraperitoneally injected with Rg1. At 24 h, 4 and 8 weeks after cell transplantation, serum sex hormone levels, oestrous cycles, ovarian pathological changes, granulosa cell (GC) apoptosis and antiapoptotic and proapoptotic protein expression in ovaries were evaluated. A chemotherapy-induced injury model of GCs was established by treatment with cisplatin in vitro to investigate the underlying mechanisms.

Results hAD-MSC transplantation significantly increased Bcl-2 expression; decreased Bax, cleaved-caspase-3, cleaved-caspase-9 and cleaved-PARP expression; and inhibited GC apoptosis in POI ovaries, which reduced ovarian injury and improved ovarian function in chemotherapy-induced POI rats; and the effects of hAD-MSC transplantation were significantly improved by Rg1 combined with hAD-MSC transplantation. Moreover, the enhanced efficacy of hAD-MSCs by Rg1 combined with hAD-MSCs in the inhibition of ovarian GC apoptosis was demonstrated in a chemotherapy injury model of GCs induced by cisplatin in vitro. The mechanisms might involve the modulatory role of Rg1 on both transplanted hAD-MSCs and GCs in the ovaries of POI rats, which indirectly and directly promoted the

†Jiali Zeng and Lanhua Wu contributed equally to this work and share first authorship.

*Correspondence:
Li Ling
304869@hospital.cqmu.edu.cn

Full list of author information is available at the end of the article

© The Author(s) 2025. **Open Access** This article is licensed under a Creative Commons Attribution-NonCommercial-NoDerivatives 4.0 International License, which permits any non-commercial use, sharing, distribution and reproduction in any medium or format, as long as you give appropriate credit to the original author(s) and the source, provide a link to the Creative Commons licence, and indicate if you modified the licensed material. You do not have permission under this licence to share adapted material derived from this article or parts of it. The images or other third party material in this article are included in the article's Creative Commons licence, unless indicated otherwise in a credit line to the material. If material is not included in the article's Creative Commons licence and your intended use is not permitted by statutory regulation or exceeds the permitted use, you will need to obtain permission directly from the copyright holder. To view a copy of this licence, visit http://creativecommons.org/licenses/by-nc-nd/4.0/.

antiapoptotic effects on ovarian GCs, respectively, and the PI3K/Akt-mitochondrial intrinsic pathway of apoptosis may be a vital target pathway involved in these processes.

Conclusion Rg1 may promote the efficacy of hAD-MSC transplantation in alleviating chemotherapy-induced POI in rats. Rg1 might be a novel adjuvant drug to promote the efficacy of MSCs in the treatment of chemotherapy-induced POI.

Keywords Ginsenoside Rg1, Human amnion-derived mesenchymal stem cells (hAD-MSCs), Premature ovarian insufficiency (POI), Chemotherapy, Apoptosis

Introduction

Premature ovarian insufficiency (POI), previously known as premature ovarian failure (POF), is a clinical syndrome characterized by the loss of ovarian activity before the age of 40 years [1]. POI can result in multiple adverse sequelae, including infertility, an increased risk of fracture, cardiovascular disease, cognitive impairment and reduced life expectancy [1]. POI affects approximately 1–4% of young women under the age of 40 years [1, 2], and chemotherapy is among the main causes of POI [3]. Exposure to chemotherapy agents may induce follicle loss, vascular damage and tissue fibrosis in ovaries and disrupt ovarian function both as an endocrine gland and as a reproductive organ [3–5]. However, POI currently has no effective treatment. Thus, exploring treatment strategies for POI is highly important.

Mesenchymal stem cells (MSCs), which exhibit both self-renewal and high plasticity [6, 7], can differentiate into osteoblasts, adipocytes and chondrocytes and secrete various cytokines and exosomes in different microenvironments [4, 8]. Human amnion-derived MSCs (hAD-MSCs) isolated from human amnions exhibit the typical characteristics of MSCs, and their isolation process is noninvasive, secure and ethically compliant [9, 10]. Thus, hAD-MSCs are regarded as potential candidate cell sources for tissue engineering and regenerative medicine [4, 10].

Thus far, studies have explored the use of MSCs to treat a variety of diseases [11, 12], and the use of MSCs as a new therapeutic approach is highly promising for POI patients [13]. Both preclinical studies in various animal models and clinical studies in humans have shown that the transplantation of MSCs can decrease ovarian injury, increase follicular development and rescue the ovarian function of POI animals and patients, indicating the promising application of MSCs for POI treatment [2, 14–16]. However, some limitations of the use of MSCs for POI treatment, such as senescence, apoptosis, low retention and a low survival rate of transplanted stem cells in ovaries (< 20%), limited or unsatisfactory efficacy in some cases, and difficulty in maintaining long-term therapeutic efficacy, may affect their clinical application [14, 17–21]. Therefore, the exploration of methods to improve the efficacy of MSC transplantation for POI treatment is necessary, and the use of MSCs in combination with pharmaceuticals can be considered a potential strategy [13].

The ginsenoside Rg1 (Rg1) is purified from the root or stem of ginseng [6]. In the human body, Rg1 regulates organ function, which is inseparable from its regulation of adult stem cells [6]. Previous studies have shown that Rg1 treatment may positively regulate the senescence, apoptosis and proliferation of MSCs in different microenvironments in vivo or in vitro [6, 22, 23]. Rg1 has extensive antiapoptotic effects on MSCs in different apoptotic models [6, 23, 24]. Liu et al. reported that Rg1 could protect human umbilical cord blood-derived stromal cells against tert-butyl hydroperoxide-induced apoptosis [25]. Luo et al. reported that Rg1 enhanced the paracrine efficacy of bone marrow MSCs (BM-MSCs) [26]. Studies have shown that appropriate concentrations of Rg1 can effectively regulate the expression and secretion of active cytokines by MSCs [6, 27]. Our previous studies also revealed that Rg1 could promote the viability, proliferation and paracrine activity and relieve the senescence of hAD-MSCs [28]. Multiple studies have shown that Rg1 can inhibit the apoptosis and senescence of MSCs and thus affect tissue repair in injured tissue and organs [6]. Bao et al. reported that compared with treatment with Rg1 alone or with BM-MSCs alone, treatment with Rg1 combined with human BM-MSCs had better antiapoptotic effects and resulted in better brain recovery in a rat cerebral ischaemia–reperfusion injury model [29]. Zheng et al. reported that Rg1 improved the survival of transplanted BM-MSCs and protected BM-MSCs from apoptosis induced by ischaemia in the arterial embolism hind limb of female rats [30]. In this study, whether Rg1 can improve the efficacy of hAD-MSC transplantation in treating rats with chemotherapy-induced POI and its mechanisms were investigated.

Materials and methods

This research complied with the Helsinki Declaration and was approved by the Ethics Committee of the Second Affiliated Hospital of Chongqing Medical University (Permit number: 2020-20).

Reagents

Foetal bovine serum (FBS), 0.25% trypsin-ethylenediaminetetraacetic acid (EDTA), Dulbecco's modified Eagle's medium/nutrient mixture F-12 (DMEM/F-12) and low-glucose DMEM (L-DMEM) were purchased from Gibco Co. (Grand Island, NY, USA). PKH26 Red Fluorescent Cell Linker Kits and collagenase II were purchased from Sigma–Aldrich (St. Louis, MO, USA). 2-(4-Amidinophenyl)–6-indolecarbamidine dihydrochloride (DAPI) was purchased from Boster Biological Technology Co., Ltd. (Wuhan, Hubei, China). Rg1 (molecular formula: C42H72O14) and cisplatin were purchased from Yuanye Bio-Technology Co., Ltd. (Shanghai, China). Enzyme-linked immunosorbent assay (ELISA) kits for anti-Müllerian hormone (AMH), E2 and FSH were purchased from Uscn Life Science (Wuhan, Hubei, China), while an ELISA kit for insulin-like growth factor-I (IGF-I) was purchased from AiFang Biological Co., Ltd. (Hunan, China). A Masson's Trichrome Staining Kit was purchased from Servicebio Technology Co., Ltd. (Wuhan, Hubei, China). A TUNEL apoptosis assay kit was purchased from Roche Applied Science (Basel, Switzerland). CD34, vascular endothelial growth factor (VEGF), vascular endothelial growth factor receptor 2 (VEGFR2), IGF-I receptor, Bcl-2, Bax, phospho-Bad (Ser136), Bcl-xL, caspase-9, cleaved-caspase-9, caspase-3, cleaved-caspase-3, cleaved-PARP, Akt and phospho-Akt antibodies were purchased from Affinity Biosciences (Changzhou, Jiangsu, China). IGF-I protein was purchased from Target Molecule Corp. (Shanghai, China). All other chemicals were purchased from the Beyotime Institute of Biotechnology (Haimen, Jiangsu, China).

Cell line

The human ovarian granulosa cell (GC) line (KGN cells) [31, 32] was purchased from Xiamen Immocell Biotechnology Co., Ltd. (Xiamen, Fujian, China) and cultured in DMEM/F-12 supplemented with 10% FBS, 100 U/ml penicillin and 100 mg/ml streptomycin at 37 °C in 5% CO_2 [32]. GCs were seeded at a density of 1×10^5 cells/ml in multiwell plates or T25 flasks (Corning, Corning, NY). When the cells reached 80–90% confluency, they were passaged at a ratio of 1:2.

Isolation, culture, identification and labelling of hAD-MSCs

Primary hAD-MSCs were isolated and cultured according to our previously published protocols [9]. hAD-MSCs isolated from human amnions exhibit the typical characteristics of MSCs, and the procedures for obtaining hAD-MSCs were noninvasive, safe and out of ethical debate, as verified by our study and other studies [4, 9, 10, 33]. Written informed consent was obtained from all the donors before the amnion was collected. Amnions were separated from the placenta of women in term pregnancy after caesarean delivery. The amnions were digested with 0.05% trypsin-EDTA and 0.75 mg/mL collagenase II in sequence. Then, the digested mixture was filtered through a 300 mesh sieve, and primary hAD-MSCs in the filtrate were obtained by centrifugation. The isolated hAD-MSCs were seeded at a density of 5×10^5/cm^2 in well plates or T25 flasks and cultured in L-DMEM supplemented with 12% FBS, 100 U/ml penicillin and 100 mg/ml streptomycin at 37 °C in 5% CO_2. When the cells reached 90–100% confluence, they were passaged at a ratio of 2:3. Third-passage hAD-MSCs were identified and labelled with PKH26 according to our previously published methods [4, 9] and were used in subsequent experiments.

Animal protocols

Female Sprague–Dawley (SD) rats were purchased from the Experimental Animal Centre of Chongqing Medical University. The work has been reported in line with the ARRIVE guidelines 2.0. All the animals were raised in a laboratory animal room with specific pathogen-free (SPF) conditions at the Experimental Animal Centre of Chongqing Medical University, which was maintained at 22 ± 2 °C, 50 ± 10% relative humidity, and a fixed 12 h light/dark cycle. The rats aged 10 to 12 weeks with normal oestrous cycles were included in the experiments.

This is an animal study in the pilot and exploratory phase [34]. The sample size was determined on the basis of our preliminary experiments [4, 5, 35, 36], literature review [37, 38] and statistical calculations [39], which have been proven adequate in terms of statistical power to detect differences in key endpoints. Additionally, the animal experiments were conducted in accordance with 3R-Refinement principles (Replacement, Reduction and Refinement) [40].

One hundred female Sprague–Dawley (SD) rats from 10 to 12 weeks of age were randomly divided into 5 groups: control, POI, Rg1, hAD-MSC treatment (hAD-MSCs) and Rg1 combined with hAD-MSC treatment (Rg1 + hAD-MSCs) groups ($n = 20$ in each group; a schematic of the animal experiments is shown in Fig. 1a). To minimize potential confounders, the rats in the different groups were treated with no fixed orders or fixed cage locations. The rats in the POI, Rg1, hAD-MSCs and Rg1 + hAD-MSCs groups were intraperitoneally injected with 2 mg/kg/day of cisplatin.

resuspended in normal saline for 6 consecutive days to establish the POI model according to our previously published protocols [41], while the rats in the control group were intraperitoneally injected with an equivalent volume of normal saline. At 24 h after the establishment of the chemotherapy-induced POI model, the rats in the hAD-MSCs and Rg1 + hAD-MSCs groups were injected with 4×10^6 PKH26-labelled hAD-MSCs via the tail vein,

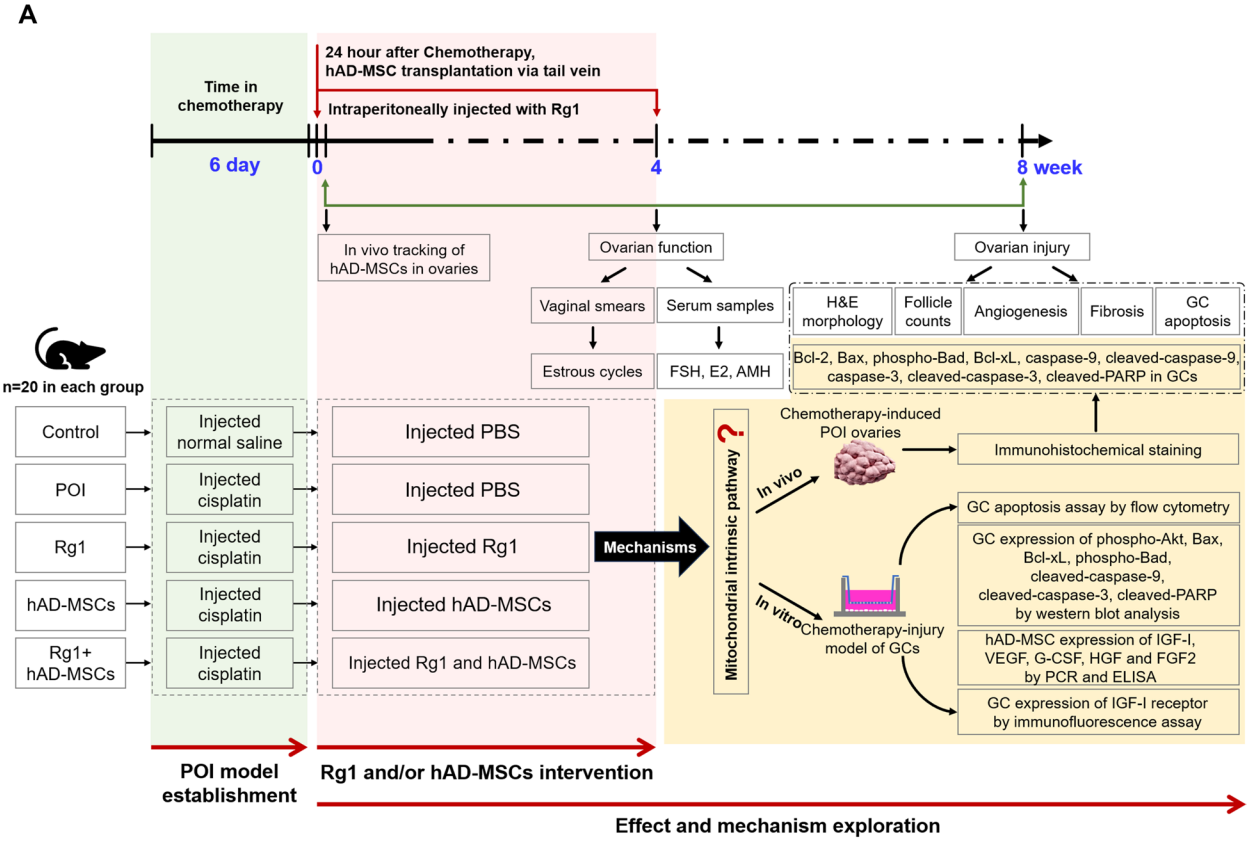


Fig. 1 (See legend on next page.)

(See figure on previous page.)

Fig. 1 Experimental protocols and schematic**. a** A schematic of the experimental procedure used to explore the effects of Rg1 combined with hAD-MSCs on chemotherapy-induced POI in rats. **b** A schematic of the experimental procedure in vitro used to explore whether Rg1 enhances the efficacy of hAD-MSCs in the inhibition of GC apoptosis in chemotherapy-induced POI ovaries by indirectly acting on hAD-MSCs or directly acting on GCs. Cell co-culture device of hAD-MSCs and GCs was constructed in vitro using Corning® Transwell® 24-mm diameter and 0.4 μm pores membrane insert of cell culture system. GCs were randomly divided into the control, cisplatin, Rg1, hAD-MSCs, Rg1 + hAD-MSCs-1, Rg1 + hAD-MSCs-2 and Rg1 + hAD-MSCs-3 groups. GCs (placed into the lower chambers of the cell co-culture devices) were treated with cisplatin followed by the treatment of hAD-MSCs (placed into the upper chambers of the cell co-culture devices) or/and Rg1 with the concentration of 10, 20, 40 or 80 ug/mL. POI, premature ovarian insufficiency; hAD-MSCs, human amnion-derived mesenchymal stem cells; GC, granulosa cell; Rg1, ginsenoside Rg1;. AMH, anti-Müllerian hormone; E2, estradiol; FSH, follicle-stimulating hormone.

whereas the rats in the Rg1 and Rg1 + hAD-MSCs groups were intraperitoneally injected with Rg1 at a dosage of 40 mg/kg/day for 28 consecutive days [42, 43]. At 24 h, 4 and 8 weeks after cell transplantation, 6 rats in each group were narcotized using sodium pentobarbital and then sacrificed, after which the ovaries and blood were collected for subsequent experiments.

Serum levels of AMH, E2 and FSH in proestrus or diestrus rats ($n = 5$ or 6) in each group at the indicated time points (0, 4 and 8 w after cell transplantation) were detected by ELISA kits according to the manufacturer's instructions.

Observation of hAD-MSCs in rat ovaries after cell transplantation

At 24 h after cell transplantation, ovarian tissue from 3 rats in each group was fixed with optimal cutting temperature (OCT) compound and made into fresh Sect. (10 μm thick) [4]. The sections were incubated with DAPI and imaged under a fluorescence microscope (Nikon Corporation, Tokyo, Japan).

Observation of oestrous cycles

Vaginal smears from 6 rats in each group were obtained at 8:30 am daily and stained with haematoxylin and eosin to observe oestrous cycles during the 1st, 4th and 8th weeks after cell transplantation. The regular oestrous cycle of rats, consisting of four sequential stages (proestrus, oestrous, metestrus and diestrus), was identified depending on the presence or absence of nucleated epithelial cells, cornified epithelium and leukocytes [44]. The irregular oestrous cycles included a prolonged oestrous cycle and an irregular duration of diestrus and/or proestrus, which were defined according to our previously published protocols [5].

Haematoxylin and Eosin (HE) staining

To observe ovarian morphology and follicle counts after hAD-MSC and/or Rg1 treatment in rats with POI, 10 ovaries from each group were collected at 8 weeks after hAD-MSC transplantation and fixed with 4% paraformaldehyde for 48 h. The ovaries were dehydrated, embedded, sectioned and stained with HE. After staining, the sections were imaged by an optical microscope (Olympus Corporation, Tokyo, Japan). Follicles were counted and categorized in every fifth section through the ovaries, which were classified as primordial, primary, secondary, preovulatory, or atretic follicles as described previously [36].

Immunohistochemical staining

Sections of ovarian tissue were incubated with specific primary antibodies against CD34, VEGF, VEGFR2, Bcl-2, Bax, phospho-Bad (Ser136), Bcl-xL, caspase-9, cleaved-caspase-9, caspase-3, cleaved-caspase-3 and cleaved-PARP; the sections were subsequently incubated with the corresponding secondary antibodies conjugated to horseradish peroxidase, stained with 3,3'-diaminobenzidine, and counterstained with haematoxylin. Then, the ovarian sections were observed under an optical microscope. The sections were analysed as described in our previously published protocols [5]: the number of positive cells (brown cells) was graded as 4 (>75%), 3 (51–75%), 2 (25–50%), 1 (5–25%) or 0 (< 5%), and the staining intensity was graded as 3 (brown), 2 (light brown), 1 (light yellow) or 0 (no colour). The total score was calculated as the sum of the two grades, which was named the immunoreactivity score (IS). Ten high-power fields (HPFs, 400×) were randomly chosen from five sections in each group for scoring. The median and range of the ISs for each group were calculated.

In addition, CD34 immunohistochemical staining of ovarian sections was used to assess microvessel density (MVD), and the MVD was measured according to the Weidner method [45, 46]. Microvessels were defined as any CD34-positive endothelium with a viable lumen, and large vessels with thick muscular walls were excluded from counting [47]. In short, the areas with the greatest number of microvessels were identified by scanning the ovarian sections in a low-power field (40×), and 9 areas with the highest density of microvessels were selected from 3 sections by two assessors in each group. Afterwards, the individual microvessels were counted in 9 fields of the HPFs (200×), the mean value of which was defined as the MVD.

Masson's trichrome staining

For the analysis of ovarian stromal fibrosis, Masson's trichrome staining was performed to stain the ovaries of each group according to the manufacturer's instructions. The fibrotic area was stained blue. ImageJ 1.42q software

was used to analyse the fibrotic area of the stained ovarian slides. The positive area ratio (%) was defined as the ratio of Masson's trichrome-stained area/total ovary area [48].

TUNEL assay

Apoptosis in ovaries was detected by a TUNEL apoptosis assay kit according to the manufacturer's instructions. Ovarian sections were observed and imaged by an optical microscope. The nuclei of apoptotic cells in the ovaries were stained dark brown.

In vitro establishment of a chemotherapy-induced injury model of GCs with cisplatin

In total, 1×10^5 cells/ml of GCs were cultured for 24 h and incubated with cisplatin to establish a chemical injury model in vitro [49, 50]. The GCs were stained with 0.1% crystal violet staining solution at 24 and 48 h after cisplatin treatment and observed under an optical microscope. The inhibition rates of GC proliferation (IRsGCP) and GC apoptosis at 24 and 48 h after cisplatin treatment were detected using a cell counting kit-8 (CCK-8) assay and flow cytometry, respectively.

Analysis of the effects of Rg1 on the viability of GCs and hAD-MSCs

In total, 5×10^3 of GCs or hAD-MSCs were seeded in 96-well plates, cultured for 2 h, and then incubated with different concentrations of Rg1 (0, 10, 20, 40–80 μg/ml) for 5 days. The viability and proliferation of GCs and hAD-MSCs were detected using a CCK-8 assay according to the manufacturer's instructions.

Analysis of the effects of Rg1 on the paracrine activity of hAD-MSCs

hAD-MSCs (1×10^5 cells/mL) were cultured in 6-well plates for 24 h and then exposed to Rg1 solution (10 μg/ml) or solvent for 24 h in the Rg1 and control groups, respectively. The expression of VEGF, granulocyte-colony stimulating factor (G-CSF), hepatocyte growth factor (HGF), IGF-I and fibroblast growth factor 2 (FGF2) in hAD-MSCs was detected by real-time quantitative polymerase chain reaction (RT-qPCR), and the primers used are listed in Supplementary Table 1. RNA samples were extracted, quantified and reverse transcribed into cDNA. RT-qPCR was performed using a CFX96 Real-Time PCR Detection System (Bio-Rad, Hercules, CA, USA) with SYBR Green Real-Time PCR Master Mix (TOYOBO Life Science). Target gene expression was determined using the $2^{-\Delta\Delta Ct}$ method. β-actin was used as an internal reference.

hAD-MSCs (1×10^5 cells/mL) were cultured in 6-well plates for 24 h and then exposed to different concentrations of Rg1 (0, 10, 20, 30, 40, 50, 60, 70, 80, 90, 100, 200–300 μg/ml) for 5 days. Then, the cell supernatant in each group was collected to measure the IGF-I level by ELISA according to the manufacturer's instructions.

Analysis of the effects of IGF-I, Rg1 and/or hAD-MSCs on the apoptosis of GCs induced by chemotherapy in vitro

To explore the mechanisms underlying the enhanced efficacy of hAD-MSC transplantation promoted by Rg1 in the inhibition of GC apoptosis induced by cisplatin in POI ovaries, we constructed a cell coculture device of hAD-MSCs and GCs in vitro using a Corning® Transwell® 24-mm diameter and 0.4 μm pore membrane insert according to the manufacturer's instructions (Corning Inc., NY, USA). The GCs were randomly divided into the control, cisplatin, Rg1, hAD-MSCs, Rg1 + hAD-MSCs-1, Rg1 + hAD-MSCs-2 and Rg1 + hAD-MSCs-3 groups (Fig. 1b). The GCs were placed into the lower chambers of the cell coculture devices in these 7 groups. The GCs were cultured for 24 h and then treated with cisplatin (5 μg/ml) for 24 h in the cisplatin, Rg1, hAD-MSCs, Rg1 + hAD-MSCs-1, Rg1 + hAD-MSCs-2 and Rg1 + hAD-MSCs-3 groups. Then, the media with cisplatin were replaced with 2 ml of fresh complete media. Afterwards, hAD-MSCs with 1 ml of media were placed into the upper chamber in the hAD-MSCs, Rg1 + hAD-MSCs-1, Rg1 + hAD-MSCs-2 and Rg1 + hAD-MSCs-3 groups, while the same volume of media without hAD-MSCs was placed into the upper chamber in the control, cisplatin and Rg1 groups. Moreover, Rg1 (10, 20, 40–80 μg/mL) was added to the upper chamber in the Rg1 + hAD-MSCs-1 and Rg1 + hAD-MSCs-3 groups, while Rg1 (10, 20, 40–80 μg/mL) was added to the lower chamber in the Rg1, Rg1 + hAD-MSCs-2 and Rg1 + hAD-MSCs-3 groups. After 24 h, the GCs were collected and incubated with annexin-V-fluorescein isothiocyanate (FITC) and propidium iodide (PI), and the apoptosis rates were detected by flow cytometry.

To confirm whether IGF-I can inhibit GC apoptosis induced by cisplatin, the GCs were divided into control, cisplatin and IGF-I (50, 100 or 200 ng/mL) groups. The GCs in the cisplatin and IGF-I groups were cultured for 24 h and then treated with cisplatin (5 μg/mL) for 24 h. Then, the medium supplemented with cisplatin was replaced with fresh complete medium, and 50, 100 or 200 ng/mL IGF-I was added to the GCs in the IGF-I groups. After 24 h, the GCs were collected, and the GC apoptosis rates were determined by flow cytometry.

To further confirm whether the enhanced efficacy of hAD-MSCs promoted by Rg1 in the inhibition of ovarian GC apoptosis induced by cisplatin depends on PI3K-Akt signalling pathways, GCs were divided into the control, cisplatin, Rg1, hAD-MSCs, Rg1 + hAD-MSCs-1, Rg1 + hAD-MSCs-1 + LY294002, IGF-I (positive control) and IGF-I + LY294002 groups. GCs in the control,

cisplatin, Rg1 (20 μg/mL), IGF-I (100 ng/mL), hAD-MSCs and Rg1 + hAD-MSCs-1 (Rg1 at 20 μg/mL) groups were treated as described above. Additionally, GCs were pretreated with LY294002 (20 μmol/L) (a specific inhibitor of the PI3K-Akt pathway) for 30 min before they were treated with Rg1 and hAD-MSCs (Rg1 at 20 μg/mL) in the Rg1 + hAD-MSCs-1 + LY294002 group or with IGF-I (100 ng/mL) in the IGF-I + LY294002 group. After 24 h, the GCs were collected, and the GC apoptosis rates were determined by flow cytometry.

Western blot analysis

To explore the molecular mechanisms underlying the enhanced efficacy of hAD-MSCs by Rg1 combined with hAD-MSCs in the inhibition of ovarian GC apoptosis induced by cisplatin, GCs were grouped and treated with cisplatin as described in Fig. 1b. Then, the medium was replaced with 2 ml of fresh medium supplemented with 2% FBS, and the cells were starved for 12 h. Afterwards, hAD-MSCs with 1 ml of media were placed in the upper chamber in the hAD-MSCs, Rg1 + hAD-MSCs-1, Rg1 + hAD-MSCs-2 and Rg1 + hAD-MSCs-3 groups, while the same volume of media without hAD-MSCs was placed in the upper chamber in the control, cisplatin and Rg1 groups. Moreover, 20 μg/mL Rg1 was added to the upper chamber in the Rg1 + hAD-MSCs-1 and Rg1 + hAD-MSCs-3 groups, while 20 μg/mL Rg1 was added to the lower chamber in the Rg1, Rg1 + hAD-MSCs-2 and Rg1 + hAD-MSCs-3 groups.

Additionally, to explore the specific interactions between Rg1 and hAD-MSCs, the GCs were divided into control, cisplatin, Rg1, hAD-MSCs, Rg1 + hAD-MSCs-1, Rg1 + hAD-MSCs-1 + LY294002, IGF-I and IGF-I + LY294002 groups. GCs in the control, cisplatin, Rg1 (20 μg/mL), IGF-I (100 ng/mL), hAD-MSCs and Rg1 + hAD-MSCs-1 (Rg1 at 20 μg/mL) groups were treated as described above, and GCs in the Rg1 + hAD-MSCs-1 + LY294002 or IGF-I + LY294002 group were pretreated with LY294002 (20 μmol/L) for 30 min, followed by treatment with Rg1 and hAD-MSCs or IGF-I.

After 24 h of treatment, the GCs were collected, and the proteins were extracted, quantified, separated by SDS–PAGE and subsequently electrotransferred to PVDF membranes (Millipore, USA). Then, the membranes were incubated with specific polyclonal primary antibodies against Bax, Bcl-2, phospho-Bad (Ser136), Bcl-xL, cleaved-caspase-9, cleaved-caspase-3, cleaved-PARP, Akt or phospho-Akt, and then with the corresponding secondary antibodies. A BeyoECL Plus kit was used for colour development according to the manufacturer's instructions.

Immunofluorescence assay

GCs in the control, cisplatin, Rg1 (20 μg/mL), hAD-MSCs and Rg1 + hAD-MSCs-1 (Rg1 at 20 μg/mL) groups were treated as described for flow cytometry and then incubated with a specific primary antibody for IGF-IR followed by a secondary antibody conjugated with DyLight549. Then, the GCs were counterstained with DAPI and imaged under a fluorescence microscope (Olympus Corporation, Tokyo, Japan). Three sections with the highest infiltration density were selected from each group. The mean fluorescence intensity of IGF-IR protein expression in the GCs of each group was calculated per 200× high-power field ($n = 6$) by Image-Pro Plus 6.0 software (Media Cybernetics, Bethesda, MD, USA).

Statistical analysis

Statistical analysis was performed using SPSS 22.0 software (IBM, NY, USA). Data with a normal distribution are shown as the means ± standard deviations and were compared using one-way analysis of variance for multiple groups or independent sample t tests for two groups. For one-way analysis of variance, least significant difference (LSD) post hoc analyses were performed, as a significant difference was observed to determine where significance was obtained. Data with skewed distributions are shown as medians and quartile ranges and were compared using nonparametric Kruskal–Wallis tests for multiple groups or Wilcoxon rank tests for two groups. Statistical significance was set at $P < 0.05$.

Results

Characterization and tracking of hAD-MSCs

The isolated cells were identified as hAD-MSCs according to our previously published protocols [9] (Fig. 2a–c). PKH26-labelled hAD-MSCs in the ovaries of POI rats were traced 24 h after cell transplantation, and red fluorescence was detected and located in the interstitium of ovarian tissue in both the Rg1 + hAD-MSCs group and the hAD-MSCs group (Fig. 2d).

Effects of Rg1 combined with hAD-MSCs on ovarian function and injury in rats with chemotherapy-induced POI

To explore the effects of Rg1 (Fig. 2e, image from PubChem) combined with hAD-MSCs on ovarian function and injury in rats with chemotherapy-induced POI, the oestrous cycle, serum levels of AMH, FSH and E2, and ovarian pathology of the rats in each group were analysed (Fig. 2f–l).

We found that 100% of rats had regular oestrous cycles in the control group, while 100% of rats had irregular oestrous cycles in the first week after chemotherapy in the POI, Rg1, hAD-MSCs and Rg1 + hAD-MSCs groups (Fig. 2f and g). The percentages of rats with regular oestrous cycles were greater in the hAD-MSCs and Rg1 + hAD-MSCs groups than in the POI group at 4 and 8 weeks after hAD-MSC transplantation (Fig. 2f and g).

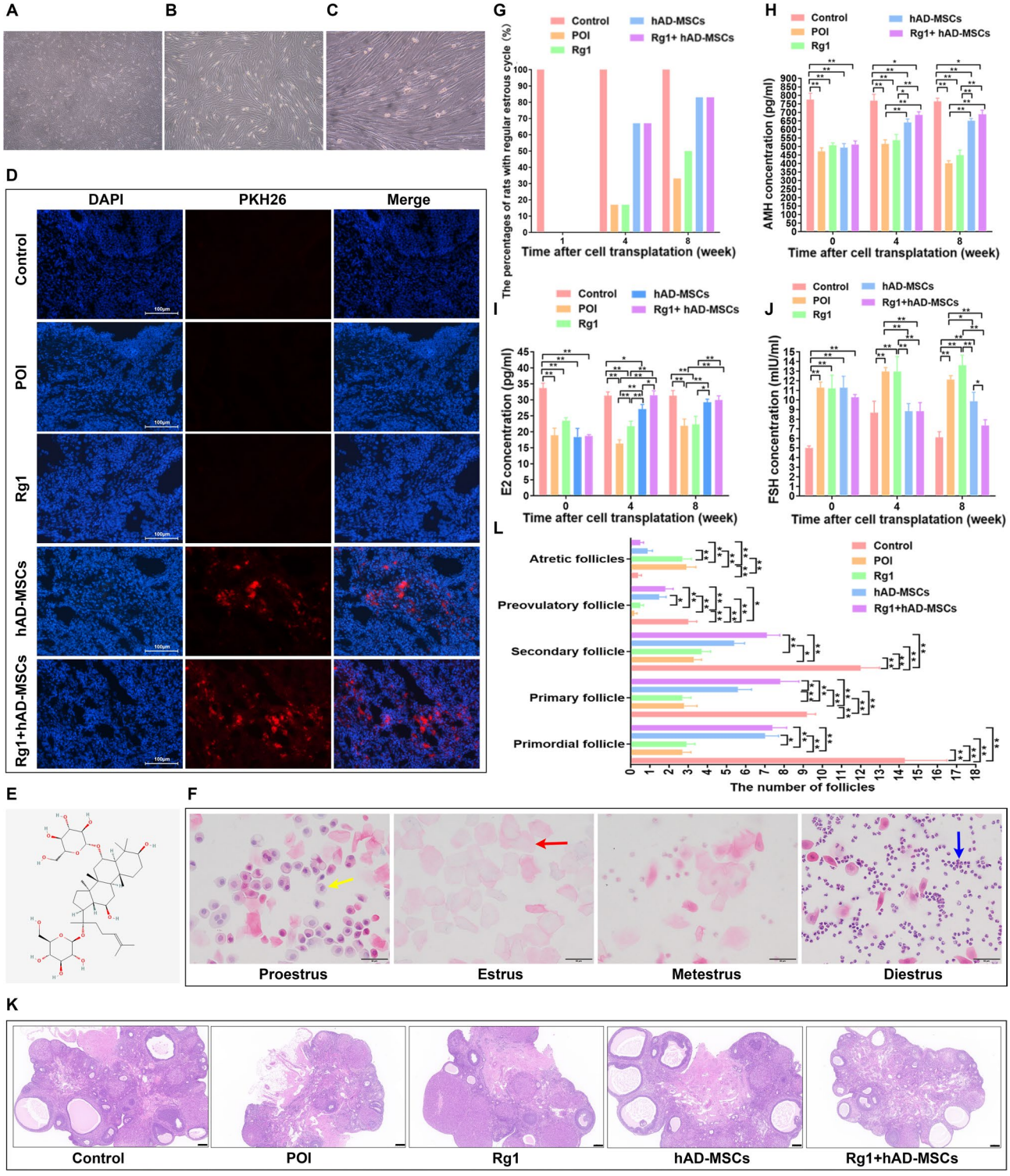


Fig. 2 (See legend on next page.)

(See figure on previous page.)

Fig. 2 Changes in ovarian function and histology of rats with chemotherapy-induced POI after Rg1 combined with hAD-MSC transplantation. **a-c** The cell morphology of hAD-MSCs (a 40×, b 100×, c 200×). **d** PKH26-labeled hAD-MSCs were observed at 24 h after transplantation in ovaries (100×, Scale bars = 100 μm) in the control, POI, Rg1, hAD-MSCs and Rg1 + hAD-MSCs groups. **e** The molecular structure of ginsenoside Rg1. **f** Vaginal smears of rats were obtained and stained by H&E, and four sequential stages of estrous cycles, proestrus, estrus, metestrus and diestrus, are shown (Scale bars = 50 μm). **g** The percentage of rats in the control, POI, Rg1, hAD-MSCs and Rg1 + hAD-MSCs groups with regular estrous cycles was detected at 1, 4, and 8 weeks after cell transplantation ($n = 6$). **h-j** Serum levels of AMH (**h**), E2 (**i**) and FSH (**j**) were evaluated at 0, 4, and 8 weeks after hAD-MSC transplantation in the control, POI, Rg1, hAD-MSCs and Rg1 + hAD-MSCs groups ($n = 5$ or 6). **k-l** Ovarian histology of rats was analyzed using HE staining (k, Scale bars = 200 μm), and the number of follicles at different stages was counted and compared (**l**) in those five groups at 8 weeks after hAD-MSC transplantation ($n = 10$). The yellow arrows indicate nucleated epithelial cells, red arrows indicate cornified epithelium and blue arrows indicate leukocytes. *$P < 0.05$ and **$P < 0.01$. AMH, anti-Müllerian hormone; E2, estradiol; FSH, follicle-stimulating hormone.

Compared with those in the control group, the AMH and E2 levels were significantly lower, while the FSH levels were significantly greater in the POI, Rg1, hAD-MSCs and Rg1 + hAD-MSCs groups at 24 h after chemotherapy ($P < 0.01$; Fig. 2h–j). AMH and E2 levels were significantly greater, whereas FSH levels were significantly lower in the hAD-MSCs and Rg1 + hAD-MSCs groups than in the POI group at 4 and 8 weeks after hAD-MSC transplantation ($P < 0.01$; Fig. 2h–j). However, there were no significant differences in the AMH, E2 or FSH levels between the POI and Rg1 groups at the eighth week after the beginning of the Rg1 treatment. AMH levels were higher in the Rg1 + hAD-MSCs group than in the hAD-MSCs group at 4 and 8 weeks after hAD-MSC transplantation. However, the difference was not significant ($P > 0.05$; Fig. 2h). Compared with that in the hAD-MSCs group, the E2 level in the Rg1 + hAD-MSCs group was significantly greater at the fourth week after hAD-MSC transplantation ($P < 0.05$; Fig. 2i), while the FSH level was significantly lower at the eighth week after hAD-MSC transplantation ($P < 0.05$; Fig. 2j).

Compared with those in the control group, the numbers of primordial, primary, secondary and preovulatory follicles in the POI group were significantly lower, whereas the number of atretic follicles was significantly greater ($P < 0.01$; Fig. 2k and l). Moreover, the numbers of primordial, primary, secondary and preovulatory follicles were significantly greater, while the numbers of atretic follicles were significantly lower in the hAD-MSCs and Rg1 + hAD-MSCs groups than in the POI group after hAD-MSC transplantation ($P < 0.05$; Fig. 2k and l). However, there was no significant difference between the POI and Rg1 groups ($P > 0.05$; Fig. 2k and l). Compared with that in the hAD-MSCs group, the number of primary follicles was significantly greater in the Rg1 + hAD-MSCs group ($P < 0.05$; Fig. 2k and l). The numbers of primordial, secondary and preovulatory follicles were also greater, while the number of atretic follicles was lower in the Rg1 + hAD-MSCs group than in the hAD-MSCs group. However, the difference was not significant ($P > 0.05$; Fig. 2k and l).

These results demonstrate that Rg1 may promote the efficacy of hAD-MSCs in improving ovarian function and reducing ovarian injury in rats with chemotherapy-induced POI.

Effects of Rg1 combined with hAD-MSCs on ovarian angiogenesis and antifibrosis in rats with chemotherapy-induced POI

To explore the effects of Rg1 combined with hAD-MSCs on ovarian angiogenesis and antifibrosis, which play important roles in repairing damaged ovaries [51], in rats with chemotherapy-induced POI, VEGF and VEGFR expression, the microvessel density and fibrosis area in the ovaries of the rats in each group were analysed (Fig. 3a–h).

Compared with those in the control group, the VEGF expression and microvessel density in the ovaries were significantly lower ($P < 0.01$; Fig. 3a, b, e and f), while the fibrosis area ratio in the ovaries was significantly greater in the POI group ($P < 0.01$; Fig. 3g and h). Moreover, compared with those in the POI group, the expressions of VEGF and microvessel density in the ovaries were significantly greater ($P < 0.01$; Fig. 3a, b, e and f), whereas the fibrosis area ratios in the ovaries were significantly lower ($P < 0.01$; Fig. 3g and h) in the hAD-MSCs and Rg1 + hAD-MSCs groups. However, the microvessel density and fibrosis area ratio did not significantly differ between the POI and Rg1 groups or between the hAD-MSCs and Rg1 + hAD-MSCs groups ($P > 0.05$; Fig. 3e, f, g and h). Compared with that in the hAD-MSCs group, the expression of VEGF in the Rg1 + hAD-MSCs group was significantly greater ($P < 0.05$; Fig. 3a and b). There was no significant difference in VEGFR expression among the five groups ($P > 0.05$; Fig. 3c and d).

These results demonstrate that Rg1 may promote the effect of hAD-MSCs on VEGF expression in ovaries and might promote ovarian angiogenesis in rats with chemotherapy-induced POI.

Effects of Rg1 combined with hAD-MSCs on ovarian GC apoptosis in rats with chemotherapy-induced POI

To further explore the effects of Rg1 combined with hAD-MSCs on ovarian apoptosis induced by chemotherapy, apoptosis and related proteins in ovaries were detected at 8 weeks after hAD-MSC transplantation (Figs. 4 and 5). The number of apoptotic GCs in the ovaries was greater in the POI group than in the control group (Fig. 4a).

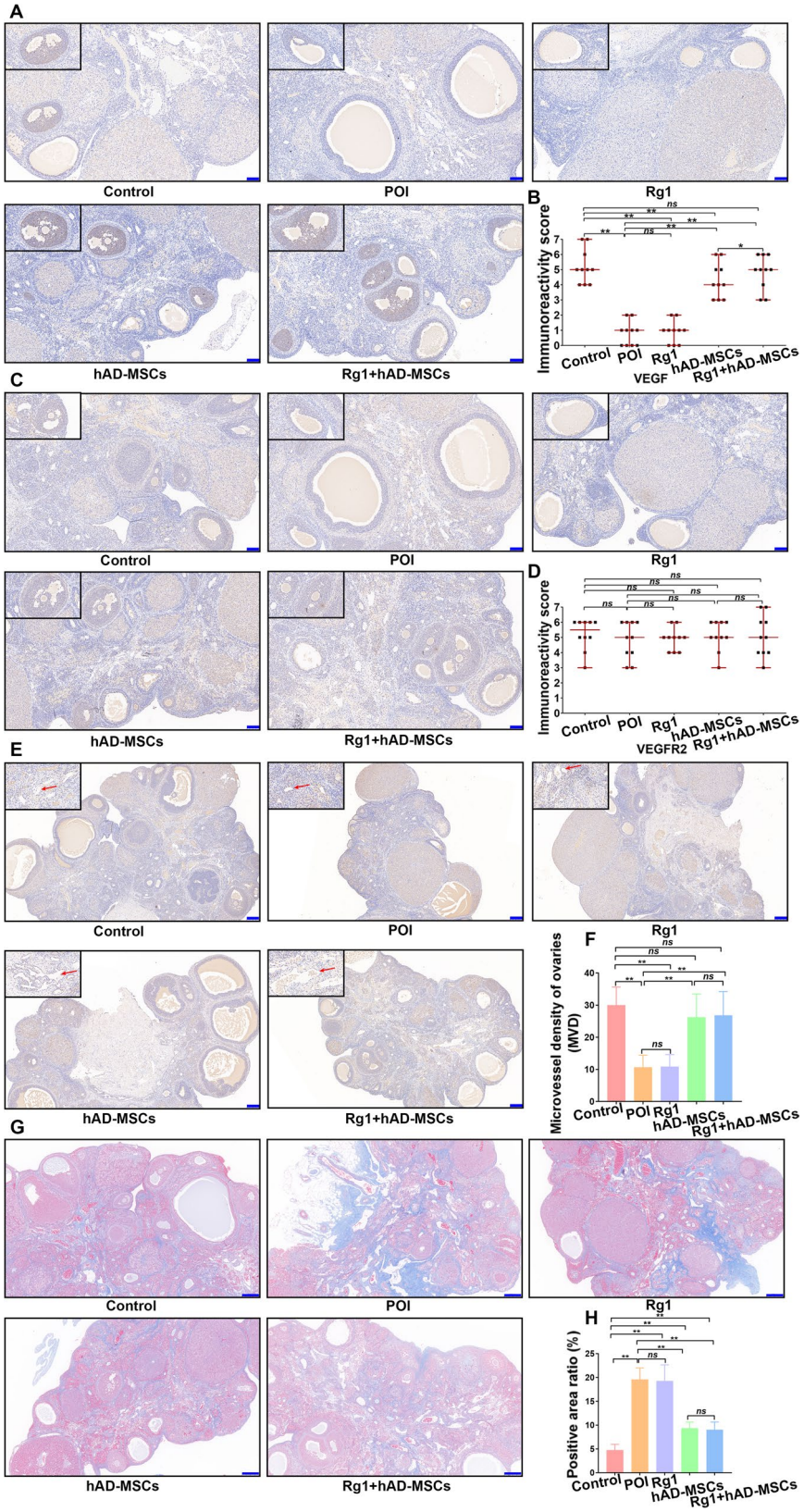


Fig. 3 (See legend on next page.)

(See figure on previous page.)

Fig. 3 Effects of Rg1 combined with hAD-MSCs on ovarian angiogenesis and anti-fibrosis in rats with chemotherapy-induced POI. **a-d** The expression levels of VEGF (**a**) and VEGFR2 (**c**) in the ovaries of the control, POI, Rg1, hAD-MSCs and Rg1 + hAD-MSCs groups were detected using immunohistochemical staining, and the semiquantitative analyses of VEGF (**b**) and VEGFR2 (**d**) levels were shown (n = 10). **e-f** The expression level of CD34 in the ovaries of each group was detected using immunohistochemical staining (**e**), and the microvessel density (MVD) based on Weidner method was counted and compared in the ovaries of those five groups (**f**, n = 9). **g-h** Ovarian fibrosis was detected by masson' s trichrome staining (**g**), and the positive area ratio (%) of ovarian fibrosis, which was defined as the ratio of Masson' s trichrome-stained area/the total ovary area, was calculated and compared (**h**) in those five groups (*n* = 6). Each dot in the graphs (**b**, **d**) represents the value obtained from ten high-power fields (HPFs) randomly chosen from five sections in each group. The bars and error bars in graphs (**b**, **d**) indicate the medians and ranges, respectively. Brown cells represent immunostained cells. The fibrotic area was stained to be blue. Representative images are shown. The red arrows indicate microvessels. **P* < 0.05 and ***P* < 0.01. Scale bars = 100 μm and 200 μm. VEGF, vascular endothelial growth factor; VEGFR2, vascular endothelial growth factor receptor 2.

Moreover, the number of apoptotic GCs in the ovaries was lower in the hAD-MSCs and Rg1 + hAD-MSCs groups than in the POI group after hAD-MSC transplantation ($P < 0.05$; Fig. 4a). Moreover, compared with that in the hAD-MSCs group, the number of apoptotic GCs in the ovaries was lower in the Rg1 + hAD-MSCs group (Fig. 4a). However, there was no obvious difference between the POI and Rg1 groups (Fig. 4a).

The expression levels of proapoptotic proteins, including Bax, cleaved-caspase-3, cleaved-caspase-9 and cleaved-PARP, were significantly greater, whereas the expression levels of the antiapoptotic proteins Bcl-2, Bcl-xL, and phospho-Bad were significantly lower in the POI group than in the control group ($P < 0.01$; Figs. 4 and 5). Moreover, the expression levels of proapoptotic proteins, including Bax, cleaved-caspase-3, cleaved-caspase-9 and cleaved-PARP, were significantly lower, while the expression levels of the antiapoptotic proteins Bcl-2, Bcl-xL and phospho-Bad were significantly higher in the hAD-MSCs and Rg1 + hAD-MSCs groups than in the POI group after hAD-MSC transplantation ($P < 0.01$; Figs. 4 and 5). Moreover, the expression levels of proapoptotic proteins, including Bax, cleaved-caspase-3, cleaved-caspase-9 and cleaved-PARP, were significantly lower, while the expression level of the antiapoptotic protein Bcl-2 was significantly higher in the Rg1 + hAD-MSCs group than in the hAD-MSCs group ($P < 0.05$; Figs. 4 and 5). Although the expression levels of the antiapoptotic proteins Bcl-xL and phospho-Bad were also greater in the Rg1 + hAD-MSCs group than in the hAD-MSCs group, the differences were not significant ($P > 0.05$; Fig. 4b and c). There were no significant differences in the expression of caspase-3 or caspase-9 among the five groups ($P > 0.05$; Fig. 5). Moreover, the expression of proapoptotic and antiapoptotic proteins did not significantly differ between the POI and Rg1 groups ($P > 0.05$; Figs. 4 and 5).

These results demonstrate that Rg1 may promote the efficacy of hAD-MSCs in the inhibition of GC apoptosis induced by chemotherapy in POI ovaries, and the pro-apoptotic intrinsic pathway might play a part in these processes.

In vitro chemotherapy-induced injury model of GCs

To investigate the mechanisms through which Rg1 enhances the efficacy of hAD-MSCs in inhibiting ovarian apoptosis and reducing ovarian injury in rats with chemotherapy-induced POI, we contrasted a cisplatin chemotherapy-induced injury model of GCs in vitro.

Compared with the control treatment (0 μg/ml cisplatin), 1 to 20 μg/mL cisplatin significantly inhibited the viability and proliferation of GCs (1, 2, 5, 10 and 20 μg/ml cisplatin; $P < 0.01$; Fig. 6a). The IRsGCPs of the cisplatin groups were significantly greater than those of the control group from 24 to 48 h after cisplatin treatment ($P < 0.01$; Fig. 6a). IRsGCP increased with time and dose in response to cisplatin.

treatment. Treatment of GCs with 5 μg/ml cisplatin for 24 h resulted in a concentration close to the half maximal inhibitory concentration (IC50) (Fig. 6a), which was selected for the subsequent experiments.

The GCs displayed a polygonal morphology (Fig. 6b). Cisplatin significantly induced the apoptosis of GCs (Fig. 6b–d). Compared with that in the control group, the GC apoptosis rate in the cisplatin group was significantly greater ($P < 0.01$; Fig. 6c–d).

Effects of Rg1 combined with hAD-MSCs on ovarian GC apoptosis induced by chemotherapy in vitro

A CCK-8 assay was performed to test the effects of Rg1 on the viability and proliferation of hAD-MSCs and GCs (Fig. 6e, f). Compared with the control treatment (0 μg/ml Rg1), Rg1 at concentrations ranging from 10 to 80 μg/mL significantly promoted the viability, proliferation and growth of hAD-MSCs and GCs in the Rg1 groups (10, 20, 40 and 80 μg/ml Rg1, $P < 0.05$; Fig. 6e, f).

To investigate whether Rg1 enhances the inhibitory efficacy of hAD-MSCs of GC apoptosis in chemotherapy-induced POI ovaries by indirectly acting on hAD-MSCs or directly acting on GCs, we constructed chemotherapy injury models of GCs, followed by coculture with hAD-MSCs and treatment with Rg1 in vitro. GC apoptosis rates were subsequently detected by flow cytometry in the control, cisplatin, Rg1, hAD-MSCs, Rg1 + hAD-MSCs-1, Rg1 + hAD-MSCs-2 and Rg1 + hAD-MSCs-3 groups (Fig. 6g). Compared with the control treatment, cisplatin significantly induced the apoptosis of GCs in the cisplatin group ($P < 0.05$; Fig. 6g, h). Compared with those in the cisplatin group, the GC apoptosis rates were significantly lower in the hAD-MSCs and Rg1 + hAD-MSCs-1,

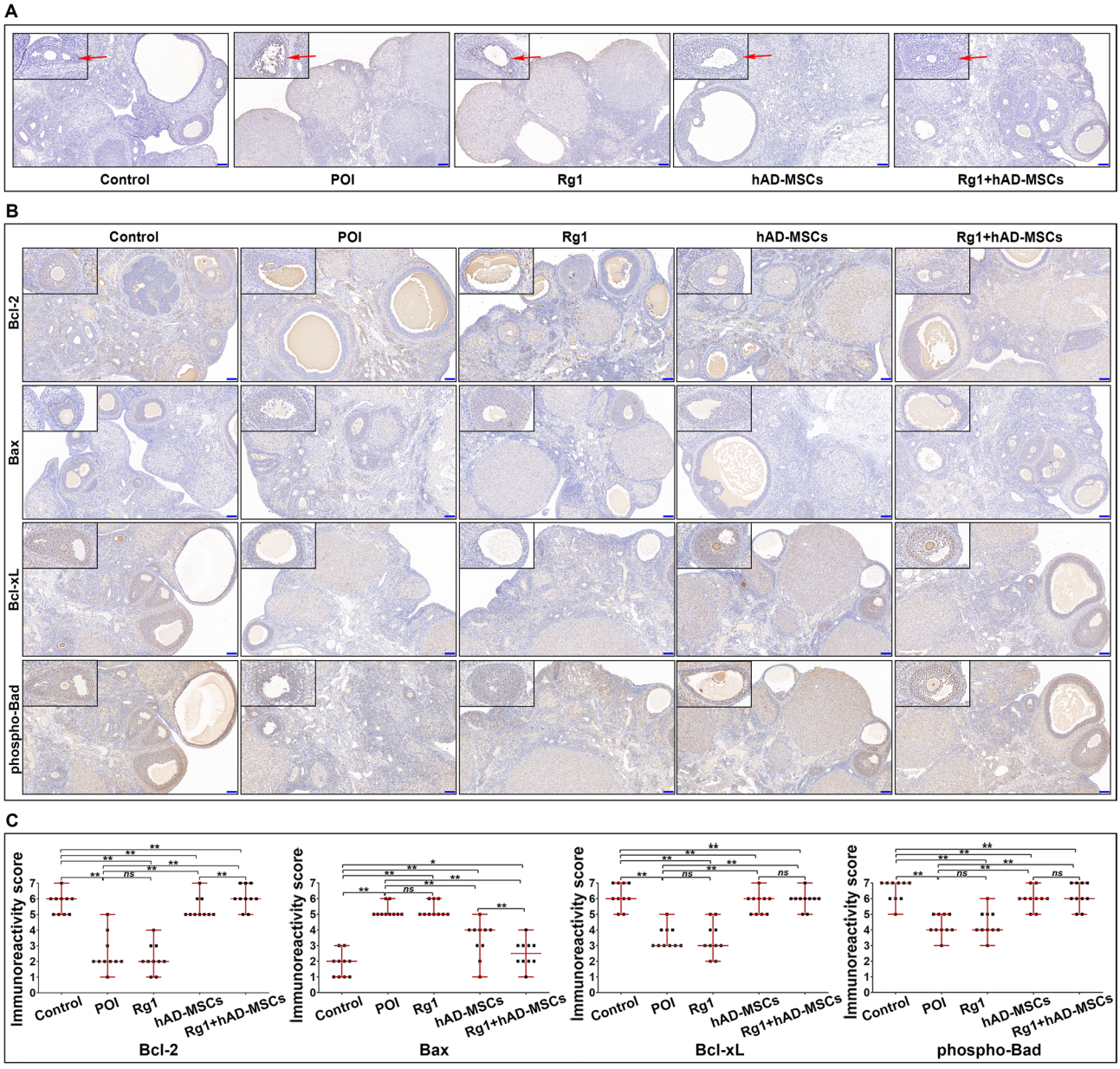


Fig. 4 Effects of Rg1 combined with hAD-MSCs on ovarian GC apoptosis and protein expression related to apoptosis in rats with chemotherapy-induced POI. **a** Ovarian GC apoptosis was detected using the TUNEL assay in the control, POI, Rg1, hAD-MSCs and Rg1 + hAD-MSCs groups. **b** The expression levels of Bcl-2, Bax, phospho-Bad (Ser136) and Bcl-xL in the ovaries of each group were detected using immunohistochemical staining. **c** Semiquantitative analyses of Bcl-2, Bax, phospho-Bad (Ser136) and Bcl-xL levels in the ovaries of each group were shown ($n = 10$). Each dot in the graphs (**c**) represents the value obtained from ten high-power fields (HPFs) randomly chosen from five sections in each group. The bars and error bars in graphs (**c**) indicate the medians and ranges, respectively. Brown cells represent immunostained cells, and red arrows indicate GCs. Representative images are shown. *$P < 0.05$ and **$P < 0.01$. Scale bars = 100 μm. GC, granulosa cell.

Rg1 + hAD-MSCs-2 and Rg1 + hAD-MSCs-3 groups ($P < 0.05$; Fig. 6g, h). Moreover, the GC apoptosis rates of the Rg1 + hAD-MSCs-1, Rg1 + hAD-MSCs-2 and Rg1 + hAD-MSCs-3 groups were significantly lower than those of the hAD-MSCs group ($P < 0.05$; Fig. 6g, h), except for the Rg1 + hAD-MSCs-1 group, which received 10 μg/ml Rg1, and the Rg1 + hAD-MSCs-2 group, which received 10 μg/ml or 80 μg/mL Rg1 ($P > 0.05$; Fig. 6g, h). Compared with those in the Rg1 + hAD-MSCs-3 groups treated with 10, 20, 40 and 80 μg/ml Rg1, the GC apoptosis rates in the Rg1 + hAD-MSCs-1 and Rg1 + hAD-MSCs-2 groups treated with 10, 20, 40 and 80 μg/ml Rg1 were significantly greater ($P < 0.05$; Fig. 6g, h). However, there was no significant difference between the Rg1 + hAD-MSCs-1 and Rg1 + hAD-MSCs-2 groups when those concentrations of Rg1 were used ($P > 0.05$;

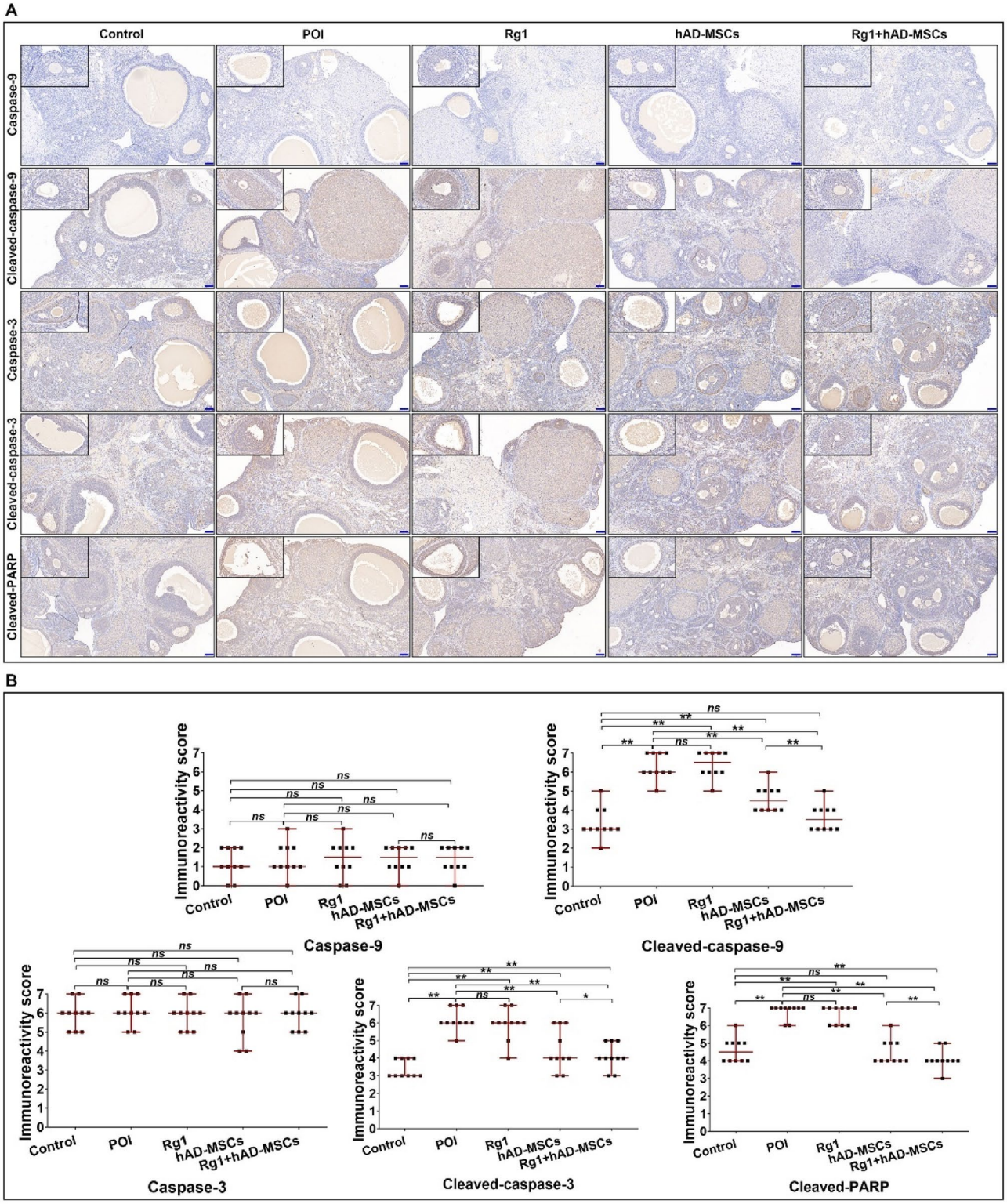


Fig. 5 Effects of Rg1 combined with hAD-MSCs on the expressions of caspase-9、cleaved-caspase-9, caspase-3, cleaved-caspase-3 and cleaved-PARP in rats with chemotherapy-induced POI. **a** The expression levels of caspase-9, cleaved-caspase-9, caspase-3, cleaved-caspase-3 and cleaved-PARP in the ovaries of the control, POI, Rg1, hAD-MSCs and Rg1 + hAD-MSCs groups were detected using immunohistochemical staining. **b** Semiquantitative analyses of caspase-9, cleaved-caspase-9, caspase-3, cleaved-caspase-3 and cleaved-PARP levels in the ovaries of each group were shown ($n = 10$). Each dot in the graphs (**b**) represents the value obtained from ten high-power fields (HPFs) randomly chosen from five sections in each group. The bars and error bars in graphs (**b**) indicate the medians and ranges, respectively. Brown cells represent immunostained cells. Representative images are shown. $^{*}P < 0.05$ and $^{**}P < 0.01$. Scale bars = 100 μm

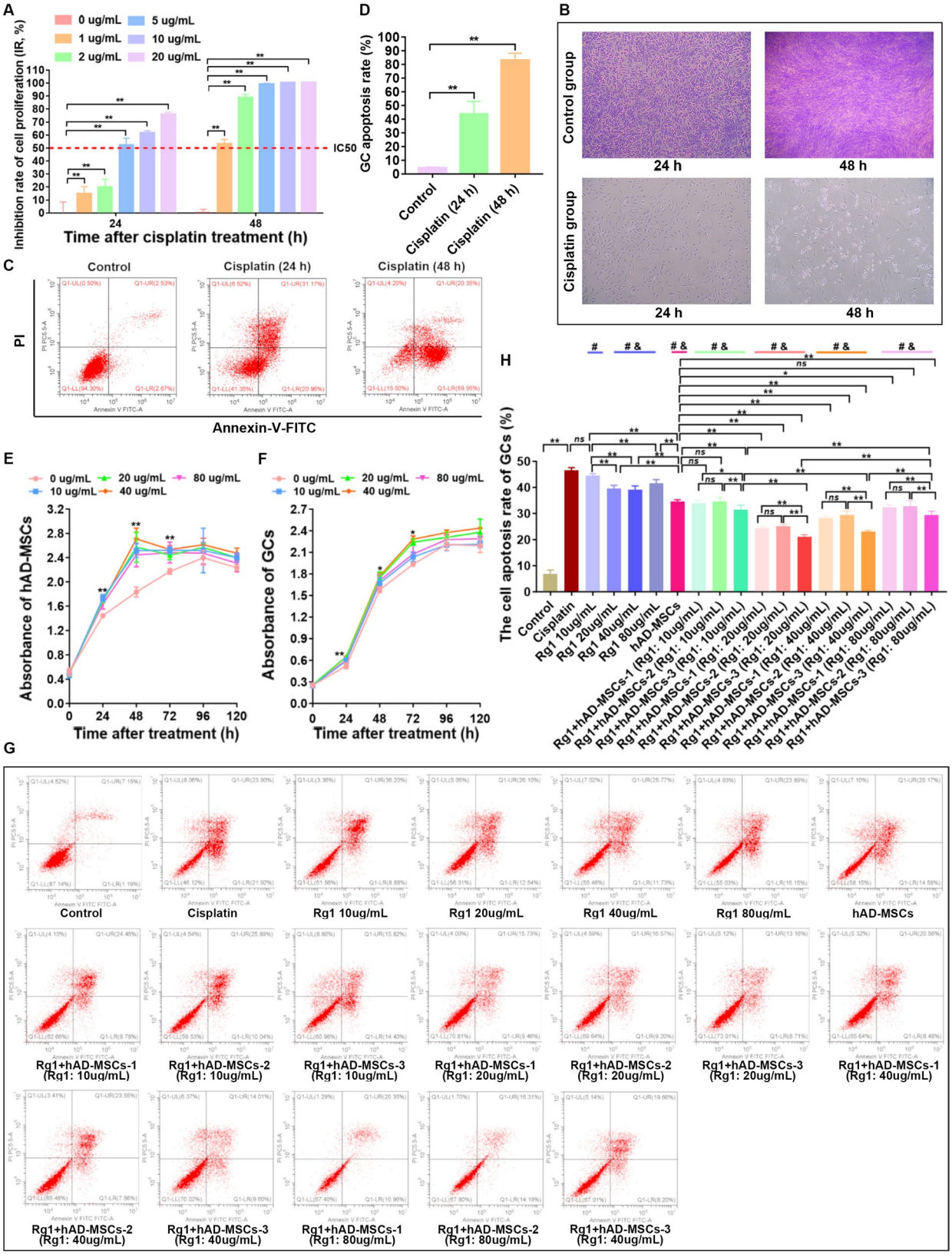


Fig. 6 (See legend on next page.)

(See figure on previous page.)

Fig. 6 Effects of Rg1 combined with hAD-MSCs on ovarian GC apoptosis induced by chemotherapy in vitro. **a** Effects of cisplatin with different concentrations (0, 1, 2, 5, 10–20 μg/ml) on the proliferation of GCs were detected using CCK-8 assay, and the inhibition rates of GC proliferation (IRsGCP) at 24 and 48 h after cisplatin treatment were calculated ($n=6$). IC50, half maximal inhibitory concentration. **b** The morphology of GCs at 24 and 48 h after cisplatin (5 μg/ml) treatment was shown in the control and cisplatin groups (100×). GCs were stained with 0.1% of Crystal Violet Staining Solution. **c-d** The GC apoptosis rates at 24 and 48 h after cisplatin (5 μg/ml) treatment in the control and cisplatin groups were analyzed (**c**) and compared (**d**) by flow cytometry ($n=3$). **e-f** Effects of Rg1 with different concentrations (0, 10, 20, 40 or 80 ug/ml) on the viability and proliferation of hAD-MSCs (**e**) and GCs (f) were detected using CCK-8 assay. Optical density (OD) values at 450 nm of each concentration at 0, 24, 48, 72, 96 and120 h after Rg1 treatment were shown ($n=6$). **g-h** The GC apoptosis rates in the control, cisplatin, Rg1 (10, 20, 40 or 80 ug/mL), hAD-MSCs, Rg1 + hAD-MSCs-1 (10, 20, 40 or 80 ug/mL of Rg1), Rg1 + hAD-MSCs-2 (10, 20, 40 or 80 ug/mL of Rg1) and Rg1 + hAD-MSCs-3 (10, 20, 40 or 80 ug/mL of Rg1) groups were analyzed (**g**) and compared (**h**) by flow cytometry ($n=3$). A representative image of three independent experiments is shown in each group. The blue, fuchsia red, green, cherry, reddish orange and pink bars in graph **h** cover and represent the Rg1 groups, hAD-MSCs group, Rg1 + hAD-MSCs groups using 10 ug/mL of Rg1, Rg1 + hAD-MSCs groups using 20 ug/mL of Rg1, Rg1 + hAD-MSCs groups using 40 ug/mL of Rg1, and Rg1 + hAD-MSCs groups using 80 ug/mL of Rg1, respectively. # represents $P<0.05$ as compared to control group; & represents $P<0.05$ as compared to cisplatin group; *ns* not significant, *$P<0.05$ and **$P<0.01$ as compared to each group. GC, granulosa cell

Fig. 6g, h). Compared with that in the Rg1 + hAD-MSCs-3 group treated with 20–40 μg/ml Rg1, the GC apoptosis rate was significantly greater in the Rg1 + hAD-MSCs-3 group treated with 10–80 μg/ml Rg1 ($P<0.05$; Fig. 6g, h). Thus, the most effective Rg1 + hAD-MSCs group with a minimum Rg1 concentration of 20 μg/ml for the inhibition of GC apoptosis was selected for subsequent molecular mechanism experiments.

These results demonstrate that Rg1 combined with hAD-MSCs can enhance the anti-apoptotic effects of hAD-MSCs on ovarian GC apoptosis induced by cisplatin, and the mechanism of this process may involve the modulatory effect of Rg1 on both hAD-MSCs and GCs.

Exploration of the molecular mechanisms of the enhanced efficacy of hAD-MSCs by Rg1 combined with hAD-MSCs in the inhibition of ovarian GC apoptosis induced by cisplatin

The pro-apoptotic intrinsic pathway, starting from mitochondria and leading to the apoptosis of ovarian follicles plays a very important role in the occurrence of POI induced by chemotherapy [3, 52]. To further explore the molecular mechanisms underlying the enhanced efficacy of hAD-MSCs promoted by Rg1 combined with hAD-MSCs in the inhibition of ovarian GC apoptosis induced by cisplatin, we randomly divided the GCs into control, cisplatin, Rg1, hAD-MSCs, Rg1 + hAD-MSCs-1, Rg1 + hAD-MSCs-2 and Rg1 + hAD-MSCs-3 groups, and the expressions of proapoptotic and antiapoptotic proteins associated with the intrinsic pathway were detected by western blot analysis in vitro.

Compared with those in the control group, the expression levels of proapoptotic proteins, including Bax, cleaved-caspase-3, cleaved-caspase-9 and cleaved-PARP,

significantly increased, while the expression levels of the antiapoptotic proteins Bcl-2 and Bcl-xL and phospho-Bad significantly decreased in the cisplatin group ($P<0.05$; Fig. 7a–f). Compared with those in the cisplatin group, the expression levels of proapoptotic proteins, including Bax, cleaved-caspase-3, cleaved-caspase-9 and cleaved-PARP, significantly decreased, while the expression levels of the antiapoptotic proteins Bcl-2, Bcl-xL and phospho-Bad significantly increased in the hAD-MSCs, Rg1 + hAD-MSCs-1, Rg1 + hAD-MSCs-2 and Rg1 + hAD-MSCs-3 groups ($P<0.05$; Fig. 7a–f). Moreover, compared with those in the hAD-MSCs group, the expression levels of proapoptotic proteins, including cleaved-caspase-3, cleaved-caspase-9 and cleaved-PARP, were further significantly decreased in the Rg1 + hAD-MSCs-3 group ($P<0.05$; Fig. 7a, b), whereas compared with those in the Rg1 + hAD-MSCs-1 or Rg1 + hAD-MSCs-2 group, the expression level of cleaved-PARP was significantly decreased in the Rg1 + hAD-MSCs-3 group ($P<0.05$; Fig. 7a, b). Compared with those in the hAD-MSCs group, the expression levels of the anti-apoptotic protein Bcl-2 and the Bcl-2/Bax ratio were significantly greater in the Rg1 + hAD-MSCs-1, Rg1 + hAD-MSCs-2 and Rg1 + hAD-MSCs-3 groups ($P<0.05$; Fig. 7c, d), while compared with those in the Rg1 + hAD-MSCs-1 and Rg1 + hAD-MSCs-2 groups, the expression levels of Bcl-2 and the Bcl-2/Bax ratio were also significantly greater in the Rg1 + hAD-MSCs-3 group ($P<0.05$; Fig. 7c, d). However, the expression levels of Bcl-xL and phospho-Bad did not significantly differ among the hAD-MSCs, Rg1 + hAD-MSCs-1, Rg1 + hAD-MSCs-2 and Rg1 + hAD-MSCs-3 groups ($P>0.05$; Fig. 7e, f).

These results show that Rg1 combined with hAD-MSCs may promote the efficacy of hAD-MSCs in reducing proapoptotic protein expression and increasing antiapoptotic protein expression associated with the proapoptotic intrinsic pathway and that the mitochondrial intrinsic pathway may be a vital target pathway involved in the enhanced efficacy of hAD-MSCs promoted by Rg1 combined with hAD-MSCs in the inhibition of ovarian GC apoptosis induced by cisplatin.

The IGF-I/IGF-IR-PI3K/Akt-mitochondrial intrinsic pathway is involved in the enhanced efficacy of hAD-MSCs promoted by Rg1 in the inhibition of ovarian GC apoptosis induced by cisplatin

In this study, Rg1 combined with hAD-MSCs could enhance the antiapoptotic effects of hAD-MSCs on ovarian GC apoptosis induced by cisplatin, and the

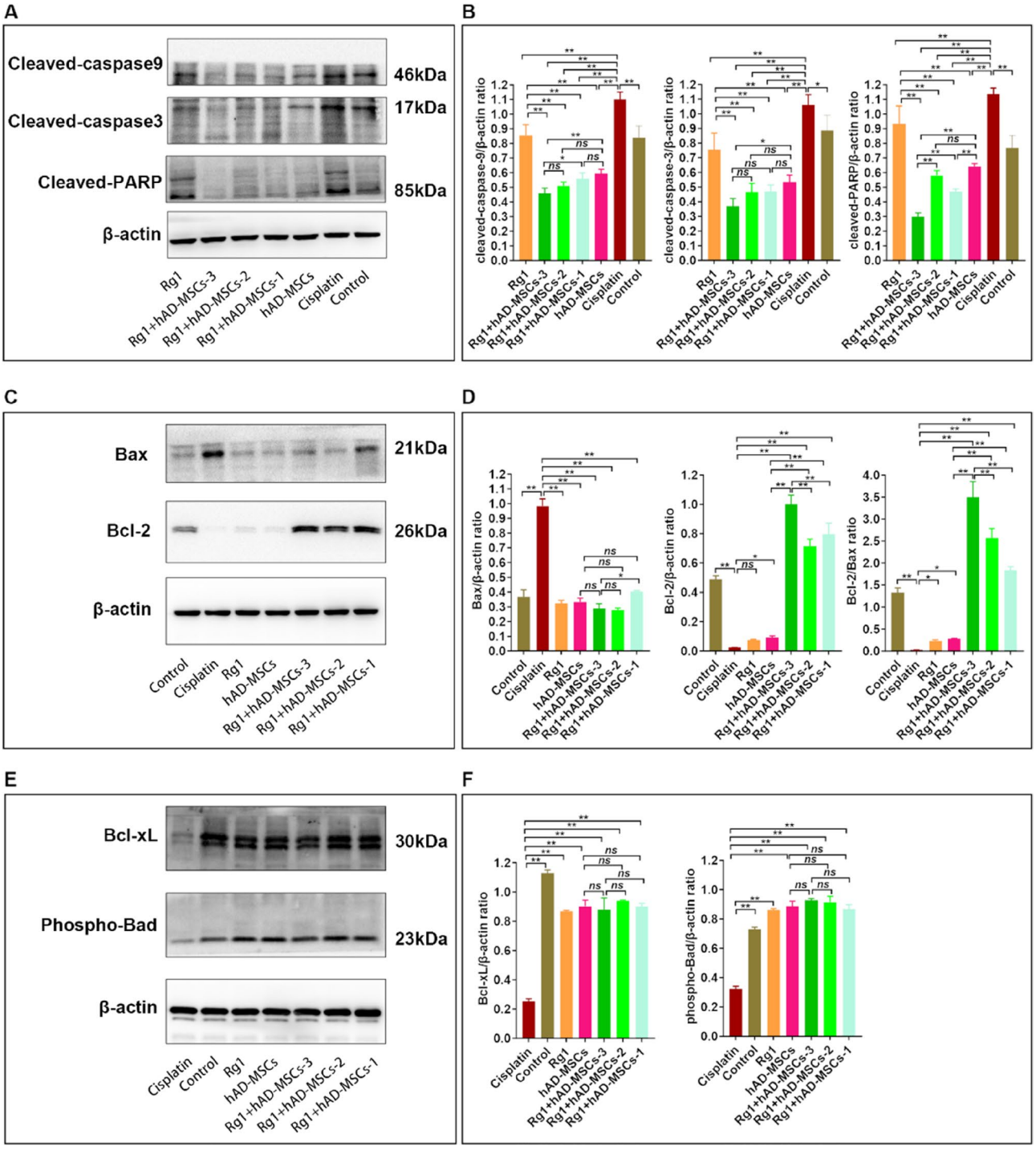


Fig. 7 Effects of Rg1 combined with hAD-MSCs on the expressions of proapoptotic and antiapoptotic protein associated with the intrinsic pathway of apoptosis in ovarian GCs injured by chemotherapy. **a-b** The expressions of cleaved-caspase-9, cleaved-caspase-3 and cleaved-PARP in GCs were analyzed (**a**) and compared (**b**) by western blot in the control, cisplatin, Rg1, hAD-MSCs, Rg1 + hAD-MSCs-1, Rg1 + hAD-MSCs-2 and Rg1 + hAD-MSCs-3 groups. **c-d** The expressions of Bax and Bcl-2 in GCs were analyzed (**c**) and compared (**d**) by western blot in those seven groups. **e-f** The expressions of Bcl-xL and phospho-Bad in GCs were analyzed (**e**) and compared (**f**) by western blot in those seven groups. $*P < 0.05$ and $**P < 0.01$

mechanism of this process may involve the modulatory effect of Rg1 on both hAD-MSCs and GCs. Therefore, we further explored the specific interactions between Rg1 and hAD-MSCs. Numerous studies have demonstrated that paracrine effects play a. vital role in the MSC-induced improvement of diseases, and the key mechanism through which MSCs restore POI is also believed to be based on their superior paracrine effects [13, 15, 51,

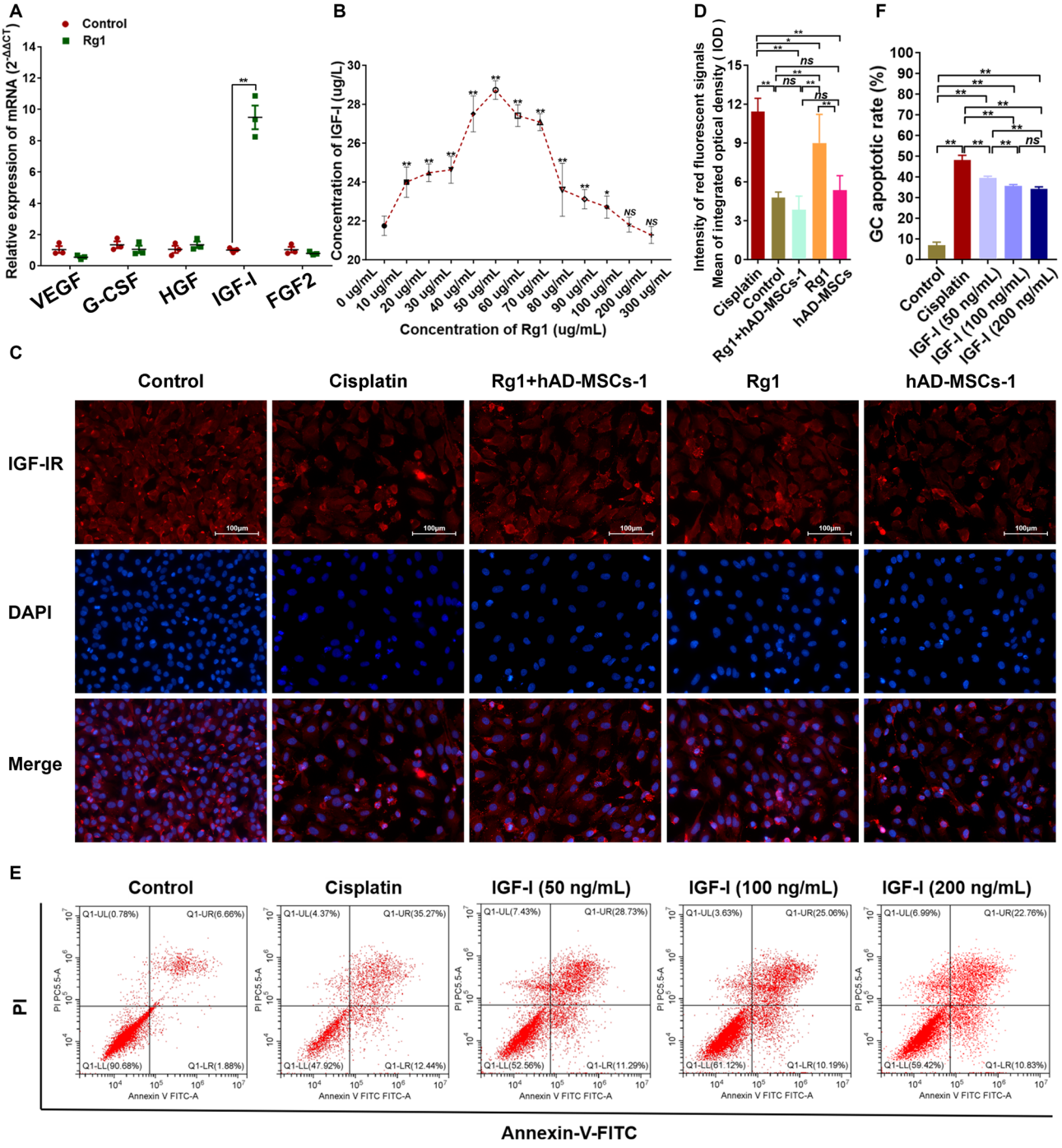


Fig. 8 Effects of Rg1 on the paracrine of hAD-MSCs and IGF-I receptor expression in GCs. **a** The relative mRNA expression levels of IGF-I, FGF2, HGF, VEGF and G-CSF in hAD-MSCs in the Rg1 and control groups were detected and compared by RT-qPCR. **b** IGF-I secreted by hAD-MSCs pretreated with various concentration of Rg1 in the cell supernatant was detected by ELISA. **, * and ns represent $P<0.01$, $P<0.05$ and $P>0.05$ as compared to 0 ug/mL of Rg1, respectively. **c-d** The protein expressions of IGF-I receptor (IGF-IR) in GCs in the control, cisplatin, Rg1, hAD-MSCs and Rg1 + hAD-MSCs-1 groups were detected (**c**) and compared (**d**) by immunofluorescence assay (200×; Scale bars = 100 μm; $n=6$). **e-f** The GC apoptosis rates in the control, cisplatin and IGF-I (50, 100 and 200 ng/mL) groups were analyzed (**e**) and compared (**f**) by flow cytometry ($n=3$). *$P<0.05$, **$P<0.01$, ns $P>0.05$. IGF-I, insulin-like growth factor-I; FGF2, fibroblast growth factor 2; HGF, hepatocyte growth factor; VEGF, vascular endothelial growth factor;. G-CSF, granulocyte-colony stimulating factor.

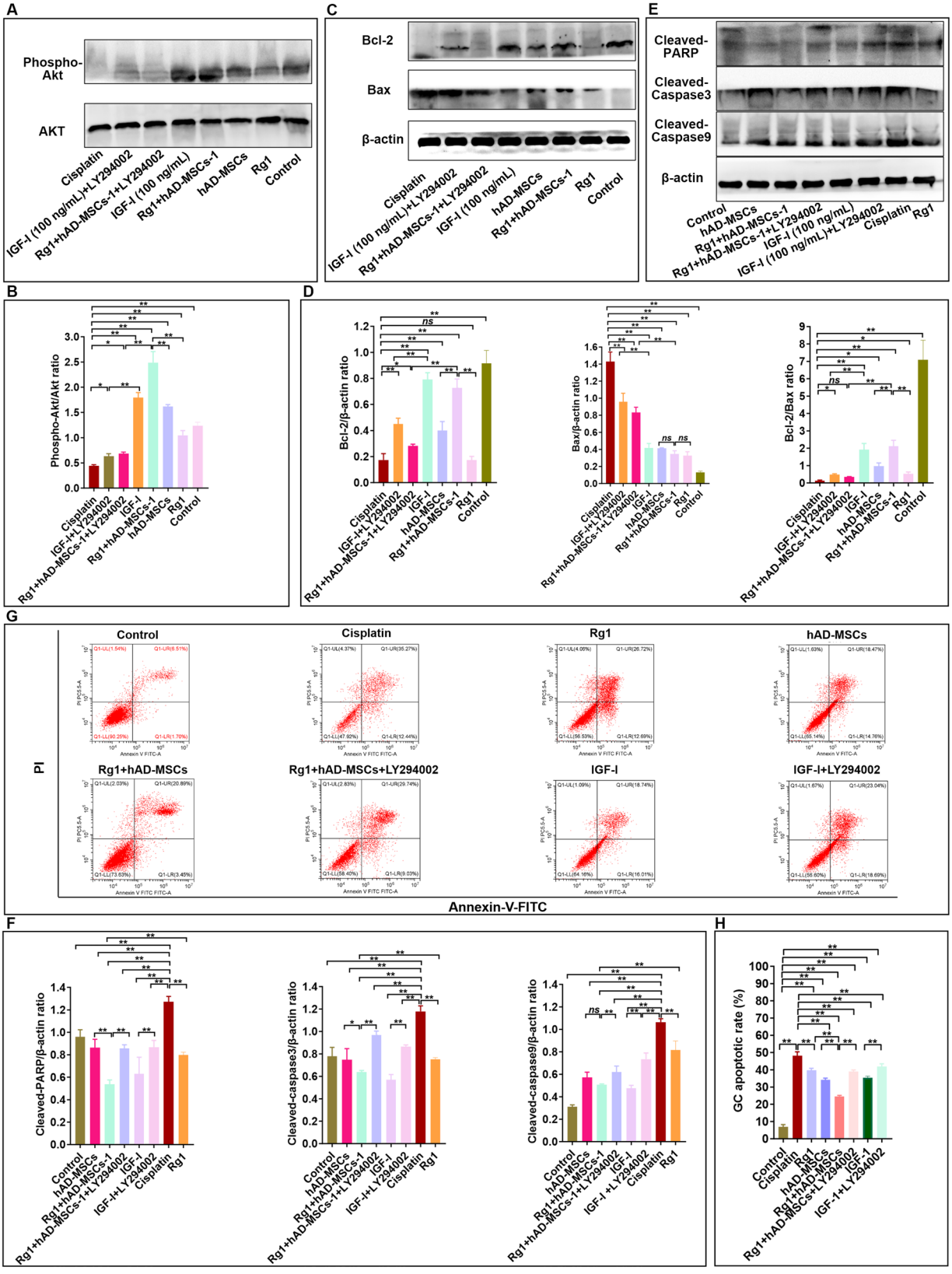


Fig. 9 (See legend on next page.)

(See figure on previous page.)

Fig. 9 PI3K/Akt-intrinsic pathway involved in the enhanced anti-apoptotic efficacy of hAD-MSCs in GCs promoted by Rg1. **a-b** The expression of phospho-Akt in GCs was analyzed (**a**) and compared (**b**) by western blot in the control, cisplatin, Rg1, hAD-MSCs, Rg1 + hAD-MSCs-1, Rg1 + hAD-MSCs-1 + LY294002, IGF-I (positive control) and IGF-I + LY294002 groups. **c-d** The expressions of Bax and Bcl-2 in GCs were analyzed (**c**) and compared (**d**) by western blot in those eight groups. **e-f** The expressions of cleaved-caspase-9, cleaved-caspase-3 and cleaved-PARP in GCs were analyzed (**a**) and compared (**b**) by western blot in those eight groups. **g-h** The GC apoptosis rates in those eight groups were analyzed (**g**) and compared (**h**) by flow cytometry ($n = 3$). *$P < 0.05$, **$P < 0.01$. IGF-I, insulin-like growth factor-I; GC, granulosa cell

53]. Thus, the effects of Rg1 on the paracrine activity of hAD-MSCs, especially growth factors secreted by hAD-MSCs, which can promote cell proliferation and reduce apoptosis [5, 54, 55], were detected by RT−qPCR and ELISA in vitro. The relative mRNA expression of IGF-I in hAD-MSCs was significantly lower in the control group than in the Rg1 group ($P < 0.01$; Fig. 8a). However, the differences in the expressions of VEGF, G-CSF, HGF and FGF2 in hAD-MSCs were not significant between the Rg1 and control groups ($P > 0.05$; Fig. 8a). Therefore, the effects of Rg1 on the secretion of IGF-I were further evaluated. Rg1 at concentrations ranging from 10 to 100 μg/mL significantly promoted the secretion of IGF-I in hAD-MSCs ($P < 0.05$; Fig. 8b). IGF-I is an important survival and growth factor [56] that can inhibit GC apoptosis and follicular atresia [57, 58].

The expression of IGF-I receptor (IGF-IR) in GCs was examined in the control, cisplatin, Rg1, hAD-MSCs and Rg1 + hAD-MSCs-1 (Rg1 only added into hAD-MSCs, Fig. 1b) groups. Red fluorescent signals, which indicated IGF-IR expression, were detected in the GCs. The mean fluorescence intensity of IGF-IR protein expression was significantly greater in the cisplatin group than in the control group ($P < 0.05$; Fig. 8c, d), which indicates that GCs treated with chemotherapy might be more sensitive to the effects of IGF-I secreted by hAD-MSCs.

To confirm whether IGF-I can inhibit GC apoptosis induced by cisplatin, GC apoptosis rates were detected by flow cytometry in the control, cisplatin and IGF-I (50, 100 and 200 ng/mL) groups. IGF-I at concentrations ranging from 50 to 200 ng/mL significantly reduced GC apoptosis induced by cisplatin ($P < 0.05$; Fig. 8e, f), and 100 ng/mL IGF-I, which was the most effective concentration among the three IGF-I groups, was selected for the subsequent experiments.

IGF-I is known as one of the most potent activators of the PI3K/Akt signalling pathway and may regulate the expression of members of the Bcl-2 family of proteins [59], inactivate caspase 9 and the apoptotic caspase protease cascade, and inhibit apoptosis [56, 60]. To further explore whether the molecular mechanisms underlying the enhanced efficacy of hAD-MSCs promoted by Rg1 in the inhibition of ovarian GC apoptosis induced by cisplatin are mediated by IGF-I/IGF-IR signalling through the PI3K/Akt signalling pathway and the intrinsic pathway of apoptosis, we randomly divided the GCs into the control, cisplatin, Rg1, hAD-MSCs, Rg1 + hAD-MSCs-1, Rg1 + hAD-MSCs-1 + LY294002, IGF-I (positive control) and IGF-I + LY294002.

groups, and phospho-Akt, proapoptotic and antiapoptotic protein expressions associated with the intrinsic pathway were detected by western blot analysis. Compared with those in the control group, the expression levels of proapoptotic proteins, including Bax, cleaved-caspase-3, cleaved-caspase-9 and cleaved-PARP, significantly increased, while the expression levels of phospho-Akt, the antiapoptotic protein Bcl-2 and the Bcl-2/Bax ratio significantly decreased in the cisplatin group ($P < 0.05$; Fig. 9a–f). Compared with those in the cisplatin group, the expression levels of these proapoptotic proteins were significantly lower in the Rg1, hAD-MSCs, Rg1 + hAD-MSCs-1 and IGF-I groups ($P < 0.05$; Fig. 9a–f), while the expression levels of phospho-Akt and the antiapoptotic protein Bcl-2 and the Bcl-2/Bax ratio were significantly greater in the hAD-MSCs, Rg1 + hAD-MSCs-1 and IGF-I groups ($P < 0.05$; Fig. 9a–f). Moreover, compared with those in the hAD-MSCs group, the expression levels of cleaved-PARP significantly decreased in the Rg1 + hAD-MSCs-1 group ($P < 0.05$; Fig. 9a–f), while the expression levels of phospho-Akt and Bcl-2 and the Bcl-2/Bax ratio significantly increased in the Rg1 + hAD-MSCs-1 group ($P < 0.05$; Fig. 9a–f). Moreover, compared with those in the Rg1 + hAD-MSCs-1 and IGF-I groups, the expression levels of cleaved-PARP significantly increased, and the expression levels of phospho-Akt and Bcl-2 and the Bcl-2/Bax ratio significantly decreased in the Rg1 + hAD-MSCs-1 + LY294002 and IGF-I + LY294002 groups, respectively ($P < 0.05$; Fig. 9a–f).

To further confirm whether the enhanced efficacy of hAD-MSCs promoted by Rg1 in the inhibition of ovarian GC apoptosis induced by cisplatin depends on PI3K-Akt signalling pathways, GCs were pretreated with the inhibitor LY294002 (20 μmol/L), and GC apoptosis rates were detected by flow cytometry. Compared with that in the hAD-MSCs group, the GC apoptosis rate in the Rg1 + hAD-MSCs-1 group decreased significantly, and this decrease was blocked by pretreatment with LY294002 ($P < 0.01$; Fig. 9g, h). The results also revealed that the GC apoptosis rates of the Rg1 + hAD-MSCs-1 + LY294002 and IGF-I + LY294002 groups were significantly greater than those of the Rg1 + hAD-MSCs-1 and IGF-I groups, respectively ($P < 0.01$; Fig. 9g, h).

These results showed that Rg1 can promote the secretion of IGF-I from hAD-MSCs and that binding of IGF-I to its receptor may induce the phosphorylation of Akt and activate the PI3K/Akt signalling pathway, subsequently regulating the expression of Bcl-2 proteins and inactivating the apoptotic caspase protease cascade of the intrinsic pathway in GCs, which may then inhibit GC apoptosis induced by cisplatin (Fig. 10). The IGF-I/IGF-IR-PI3K/Akt-mitochondrial intrinsic pathway might be involved in the enhanced efficacy of hAD-MSCs promoted by Rg1 in the inhibition of ovarian GC apoptosis induced by cisplatin.

Discussion

There is no specific or effective treatment for POI [61]. Studies have reported that MSCs have great potential for alleviating POI both in animal experiments and in preclinical and clinical studies [53]. Although MSC transplantation has shown great potential for ameliorating ovarian function in animal models and humans with POI, some limitations still exist, and its efficacy needs to be further improved [14, 17–21]. Previous studies have shown that Rg1 treatment may promote proliferation and paracrine activity and relieve the senescence and apoptosis of MSCs in different microenvironments in vivo or in vitro [6, 22, 23, 26], enhancing the efficacy of MSCs in the treatment of some diseases, such as radiation-induced intestinal injury, arterial embolism and cerebral ischaemia–reperfusion injury, in animal models [26, 29, 30]. Therefore, in this study, we explored the effects of Rg1 combined with hAD-MSCs on chemotherapy-induced POI. We found that compared with hAD-MSC transplantation, Rg1 combined with hAD-MSC transplantation was more advantageous for improving ovarian function and reducing ovarian injury in rats with chemotherapy-induced POI. Rg1 may promote the efficacy of hAD-MSCs in POI treatment.

Although the underlying mechanism of chemotherapy-associated POI is not fully understood, the DNA damage to and apoptosis of ovarian follicles induced by chemotherapy agents may cause exhaustion of available follicle deposits in ovaries and POI [3]. Apoptosis is considered one of the most important pathogenesis mechanisms of chemotherapy-induced POI [62, 63]. The high apoptosis rate of GCs is correlated with follicle reduction and ovarian dysfunction, which are the critical pathogenesis mechanisms of POI [53]. In our study, we found that the number of apoptotic GCs and atretic follicles was clearly greater in the ovaries of the POI group than in those of the control group. GC apoptosis contributes to follicular atresia and accelerates the progression of chemotherapy-induced POI [64–66]. Therefore, enhancing the antiapoptotic capacity of GCs can restore GC function and effectively ameliorate chemotherapy-induced ovarian damage [15]. MSC-based treatment has been shown to restore ovarian function in POI animal models through the inhibition of excessive GC apoptosis and follicular atresia [18, 53, 67]. Accordingly, if the apoptosis rates of GCs are associated with ovarian function, their regulation may improve the efficacy of MSCs in POI treatment [53]. In this study, we revealed that Rg1 combined with hAD-MSCs enhanced the efficacy of hAD-MSCs in the inhibition of GC apoptosis induced by chemotherapy in POI ovaries. Therefore, we speculated that the efficacy of hAD-MSCs in chemotherapy-induced POI treatment enhanced by Rg1 combined with hAD-MSCs might occur through the promotion of inhibitory effects on ovarian GC apoptosis. Moreover, this speculation was further proven through our in vitro experiments. Rg1 combined with hAD-MSCs can enhance the antiapoptotic effects of hAD-MSCs on ovarian GC apoptosis induced by cisplatin through the modulatory effect of Rg1 on both hAD-MSCs and GCs, and the underlying molecular mechanisms were further explored.

The pro-apoptotic intrinsic pathway, starting from mitochondria and leading to the apoptosis of ovarian follicles, plays a very important role in the occurrence of POI induced by chemotherapy [3, 52]. Activation of the pro-apoptotic intrinsic pathway is primarily regulated by the Bcl-2 family, among which pro- and antiapoptotic molecules are the most common markers of apoptosis [68]. The Bcl-2 family plays important roles in regulating the apoptosis of ovarian GCs at all stages of follicular growth and development [68] and determining the fate of ovarian GCs and follicles [4, 69]. Studies have shown that Bax expression is significantly increased while Bcl-2 expression is significantly decreased in rats with chemotherapy-induced POI [4, 5, 70]. Wang et al. reported that Bcl-xL expression was decreased in rats with POI [71]. Bad is expressed in ovarian GCs and leads to increased apoptosis [72]. We found that the expression levels of the proapoptotic proteins Bax and the caspase family significantly increased, whereas the expression levels of the antiapoptotic proteins Bcl-2, Bcl-xL, and phospho-Bad significantly decreased in the ovarian GCs of rats with chemotherapy-induced POI. These results were also proven in a chemotherapy injury model of GCs induced by cisplatin in vitro. All the results both in vivo and in vitro showed that the pro-apoptotic intrinsic pathway might play a very important role in the occurrence of POI induced by chemotherapy, which is in accordance with the findings of other studies [3, 52].

The antiapoptotic effects of MSCs in POI ovaries are related to the regulation of apoptosis-related genes, including Bcl-2, Bax and caspase-3 [13, 51, 73]. Studies have shown that MSC transplantation may inhibit GC apoptosis and improve ovarian function by releasing growth factors and upregulating Bcl-2 expression

[21, 51, 74]. Bahrehbar et al. reported significant downregulation of caspase-3 expression and upregulation of Bcl-2 expression in ovaries following the transplantation of embryonic stem cell-derived MSCs in a POI mouse model [21]. Huang et al. reported that MSCs can restore the ovarian function of mice with chemotherapy-induced POI through increasing the expression of Bcl-2 and survivin and repressing the expressions of caspase-3 and caspase-9 [75]. Deng et al. reported that human umbilical cord MSC transplantation significantly increased Bcl-xl protein expression, inhibited Bax protein expression and had antiapoptotic effects in chemotherapy-induced POI mice, which reduced ovary injury and improved ovarian function in POI mice [76]. These results indicate that the intrinsic pathway plays an important role in MSC-mediated therapy for chemotherapy-induced POI. In this study, we also revealed that hAD-MSCs promoted Bcl-2 protein expression and inhibited Bax, cleaved-caspase-3, cleaved-caspase-9 and cleaved-PARP expressions in the ovaries of rats with chemotherapy-induced POI. Furthermore, Rg1 combined with hAD-MSCs significantly promoted the efficacy of hAD-MSCs in terms of these effects. Our results demonstrate that the mitochondrial intrinsic pathway may be a vital target involved in the enhanced efficacy of hAD-MSCs promoted by Rg1 combined with hAD-MSCs in the inhibition of ovarian GC apoptosis induced by chemotherapy in POI rats.

In this study, it was found that Rg1 combined with hAD-MSCs could enhance the antiapoptotic effects of hAD-MSCs on ovarian GC apoptosis induced by cisplatin, and the mechanism of this process may involve the modulatory effect of Rg1 on both hAD-MSCs and GCs. Therefore, we further explored the specific interactions between Rg1 and hAD-MSCs. Current studies have demonstrated that MSCs can secrete a variety of growth factors, including VEGF, IGF-1, HGF, FGF2 and G-CSF [15, 51]. These molecules play important anti-apoptotic, anti-inflammatory, antifibrotic, antiangiogenic and immunomodulatory roles, thus improving the local microenvironment and promoting the repair of damaged tissues [51]. Many studies have demonstrated that the migration of MSCs to injured POI ovaries can improve chemotherapy-induced ovarian injury and restore ovarian function via paracrine effects [15, 51, 53]. MSC transplantation may inhibit GC apoptosis and improve ovarian function through the release of IGF-1, VEGF, FGF-2 and HGF [19, 21, 51, 74, 77–79]. Our previous studies also demonstrated that hAD-MSC transplantation could improve ovarian function in rats with chemotherapy-induced POI at least partly through a paracrine mechanism. The presence of a paracrine mechanism accounting for the hAD-MSC-mediated recovery of ovarian function might be attributed to the secretion of the growth factors FGF2, IGF-1, HGF, and VEGF by hAD-MSCs [5]. Therefore, we focused on the effects of Rg1 on the paracrine activity of hAD-MSCs and reported that Rg1 significantly promoted the expression and secretion of IGF-I in hAD-MSCs. Moreover, we found that IGF-IR was not only expressed in GCs but also expressed at higher levels in GCs after treatment with cisplatin, which might enhance the efficacy of IGF-I secreted by hAD-MSCs in GCs.

IGF-I is an important survival factor for GCs [56] and can inhibit their apoptosis [80–82]. Bencomo, E [83] and Yu Y, et al. [84] reported that IGF-I significantly reduced the number of apoptotic GC cells in vitro. IGF-I is critical for ovarian follicle growth, development and function [56, 80] and serves as a critical intrafollicular survival factor [56]. Studies have demonstrated that IGF-I supports follicular development by enhancing GC survival [56], whereas IGF-I might be involved in controlling apoptosis in GCs during follicular atresia [57]. Studies have shown that genetically engineered mice lacking IGF-I are infertile [80, 85]. MSCs have been shown to inhibit GC apoptosis in a mammalian model with POI through the IGF-1 pathway [58]. Gabr et al. reported significantly higher IGF-1 levels in the ovaries of rats with chemotherapy-induced POI after bone marrow-derived MSC (BMMSC) transplantation in the MSC transplantation group than in the control and chemotherapy groups [86], which partially improved ovarian function [86]. Thus, we speculated that the promotion of IGF-I secretion by Rg1 from hAD-MSCs might be associated with the enhanced efficacy of hAD-MSCs by Rg1 in the inhibition of ovarian GC apoptosis induced by cisplatin.

PI3K is a major downstream effector of IGF-I signalling [56]. IGF-I, a stimulator of proliferation and an inhibitor of apoptosis, is known as one of the most potent activators of the PI3K/Akt signalling pathway. Compelling evidence has indicated that Akt acts as a central mediator of IGF-I-mediated cell survival [87, 88]. PI3K/Akt signalling also serves as a functional survival pathway in the ovary and is involved in IGF-I-mediated cell survival in GCs [56]. IGF-I protects GCs from apoptosis through activation of the PI3K/Akt pathway [80]. Studies have demonstrated that IGF-I generally binds to the IGF-I receptor and activates the PI3K/Akt signalling pathway in GCs, which may inhibit GC apoptosis and possibly improve the structure and function of injured ovaries [56, 86, 89, 90], while inhibition of this pathway leads to GC apoptosis [56]. If the activity of the PI3K/Akt pathway is abnormally blocked, the development of primordial follicles is inhibited, which leads to the progression of POI [13, 68, 91]. The intrinsic pathway of apoptosis plays an important role in MSC-mediated therapy for chemotherapy-induced POI [13, 21, 51, 73–75]. The anti-apoptotic effects of MSCs in POI ovaries are related to the regulation of apoptosis-related genes in the intrinsic

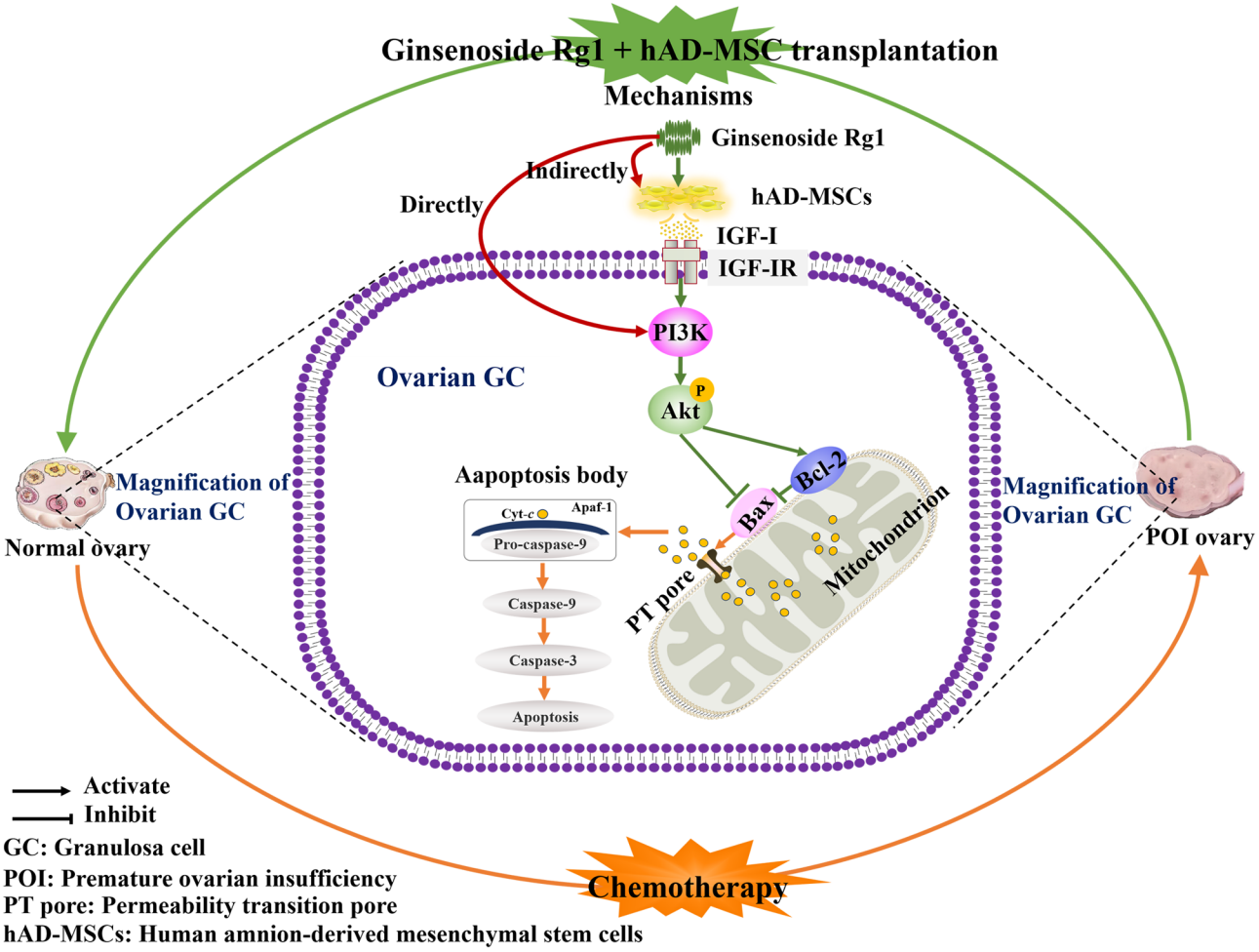


Fig. 10 Mechanism diagram. Rg1 combined with hAD-MSCs might promote the efficacy of hAD-MSCs in alleviating chemotherapy-induced POI by Rg1 indirectly and directly inhibiting GC apoptosis induced by cisplatin via regulating PI3K/Akt-mitochondrial intrinsic pathway

pathway, including Bcl-2, Bax, and caspase-3 [13]. PI3K/Akt signalling may regulate the expression of proteins of the members of the Bcl-2 family [59]. Akt has been shown to phosphorylate and inactivate caspase-9 [60], resulting in the inhibition of the apoptotic caspase protease cascade and the repression of apoptosis [56, 60]. In this study, compared with those in the hAD-MSCs group, the expression levels of phospho-Akt and Bcl-2 and the Bcl-2/Bax ratio were significantly increased, while the expression levels of cleaved-PARP and GC apoptosis were significantly decreased in the chemotherapy injury-induced model of GCs with cisplatin in vitro via Rg1 treatment with hAD-MSCs in the Rg1 + hAD-MSCs-1 group, where Rg1 promoted the secretion of IGF-I in hAD-MSCs. These effects were blocked by pretreatment with LY294002, a specific inhibitor of the PI3K-Akt pathway in GCs, which is similar to the effects of IGF-I on GCs. Therefore, the enhanced efficacy of hAD-MSCs promoted by Rg1 in the inhibition of ovarian GC apoptosis induced by cisplatin might be mediated by IGF-I/IGF-IR signalling through the PI3K/Akt-mitochondrial intrinsic pathway (Fig. 10).

In addition, in this study, we tested the effects of Rg1 on GC apoptosis induced by cisplatin in vitro. Rg1 at concentrations of 20, 40–80 μg/mL, except 10 μg/ml, significantly inhibited GC apoptosis induced by cisplatin. Additionally, Rg1 significantly promoted phospho-Akt expression; reduced Bax, cleaved-caspase-3, cleaved-caspase-9 and cleaved-PARP expression; and increased the Bcl-2/Bax ratio, which activated PI3K/Akt signalling and regulated the mitochondrial intrinsic pathway in GCs injured by chemotherapy. These results also demonstrated that the PI3K/Akt-intrinsic pathway might be involved in the efficacy of Rg1 in the inhibition of ovarian GC apoptosis induced by cisplatin (Fig. 10). These effects of Rg1 were also demonstrated in other cells. Studies have shown that the PI3K/Akt signalling pathway is likely the primary signalling pathway regulated by Rg1

[92], and Rg1 can effectively activate the PI3K/Akt signalling pathway in various cells to protect them from injury and apoptosis [92–94]. Zhong et al. reported that Rg1 reduced alveolar epithelial apoptosis by activating the PI3K/Akt signalling pathway, increasing the Bcl-2/Bax protein expression ratio, and decreasing the high expression of cleaved caspase-3 [92]. Cao et al. reported that Rg1 increased the ratio of Bcl-2/Bax and inhibited Bax translocation-mediated mitochondrial apoptosis in haematopoietic stem cells [95]. Xu et al. reported that Rg1 inhibited the high expression of Bax, caspase-3 and caspase-9 in human articular chondrocytes (HACs), which inhibited the apoptosis of HACs by inhibiting mitochondrial pathway apoptosis [96].

There were several limitations in this study. First, in the in vivo studies, we used only the concentration of Rg1 according to previously published methods by our team [42, 43]. We found that the use of Rg1 alone did not significantly inhibit GC apoptosis or improve ovarian function in rats with chemotherapy-induced POI. However, in vitro, we used multiple concentrations of Rg1 and reported that, in addition to 10 μg/ml Rg1, all the other concentrations of Rg1 significantly inhibited chemotherapy-induced GC apoptosis. Hence, other Rg1 concentrations for the treatment of chemotherapy-induced POI in vivo will be explored in our subsequent experiments. Second, the efficacy and safety of Rg1 and hAD-MSCs were observed in this study, and no obvious side effects caused by Rg1 or hAD-MSCs were observed, including immune responses in ovaries and tumorigenic risks in rats after treatment, which is in accordance with the findings of other studies [14, 97, 98]. However, this is not a long-term observation, and follow-up studies should be performed to assess the sustainability of ovarian function and long-term safety related to the repeated use of Rg1 and hAD-MSC transplantation. Third, this is a preliminary study, and more detailed molecular mechanisms need to be further investigated.

Conclusions

Rg1 combined with hAD-MSC transplantation may promote the efficacy of hAD-MSC transplantation in improving ovarian function and reducing ovarian injury in rats with chemotherapy-induced POI. The mechanisms might involve the modulatory role of Rg1 on both transplanted hAD-MSCs and GCs in the ovaries of POI rats, which indirectly and directly promote antiapoptotic effects on ovarian GCs, respectively, and the PI3K/Akt-mitochondrial intrinsic pathway of apoptosis may be a vital target pathway involved in these processes. These findings suggest that Rg1 might be a novel adjuvant drug to promote the efficacy of MSCs in the treatment of patients with chemotherapy-induced POI.

Abbreviations

POI	Premature ovarian insufficiency
MSCs	Mesenchymal stem cells
hAD-MSCs	Human amnion-derived mesenchymal stem cells
POF	Premature ovarian failure
Rg1	Ginsenoside Rg1
BM-MSCs	Bone marrow mesenchymal stem cells
UC-MSCs	human umbilical mesenchymal stem cells
L-DMEM	Dulbecco's modified eagle medium low-glucose
DMEM/F-12	Dulbecco's Modified Eagle Medium/Nutrient Mixture F-12
FBS	Fetal bovine serum
CCK-8	Cell Counting Kit-8
AMH	Anti-Müllerian hormone
E2	Estradiol
FSH	Follicle-stimulating hormone
DAPI	2-(4-amidinophenyl)-6-indolecarbamidine dihydrochloride
OD	Optical density
SD	Sprague-Dawley
HE	Hematoxylin and eosin
ELISA	Enzyme-linked immunosorbent assay
ADM	Adipogenic differentiation medium
ODM	Osteogenic differentiation medium
CDM	Chondrogenic differentiation medium
VEGF	Vascular endothelial growth factor
VEGFR2	Vascular endothelial growth factor receptor 2
IS	Immunoreactivity score
GCs	Granulosa cells
HE	Hematoxylin and eosin
HPFs	High-power fields
MVD	Microvessel density
IRsGCP	Inhibition rates of GC proliferation
FITC	Annexin-V-fluorescein isothiocyanate
PI	Propidium iodide
APAF-1	Apoptosis-activating factor
VDAC	Voltage-dependent anion channel
PARP	Poly ADP-ribose polymerase
IGF-I	Insulin-like growth factor-I
G-CSF	Granulocyte-colony stimulating factor
HGF	Hepatocyte growth factor
FGF2	Fibroblast growth factor 2

Supplementary Information

The online version contains supplementary material available at https://doi.org/10.1186/s13048-025-01886-x.

Supplementary Material 1.

Supplementary Material 2.

Supplementary Material 3.

Supplementary Material 4.

Supplementary Material 5.

Supplementary Material 6.

Supplementary Material 7.

Supplementary Material 8.

Supplementary Material 9.

Supplementary Material 10.

Supplementary Material 11.

Supplementary Material 12.

Supplementary Material 13.

Supplementary Material 14.

Supplementary Material 15.

Supplementary Material 16.

Supplementary Material 17.

Supplementary Material 18.

Supplementary Material 19.

Supplementary Material 20.

Acknowledgements
We thank the Laboratory of Stem Cell and Tissue Engineering of Chongqing Medical University for their technical assistance. The authors declare that we have not use AI-generated work in this manuscript.

Authors' contributions
Conceived and designed the experiments: Li Ling.Literature search: Li Ling, Jiali Zeng, Lanhua Wu.Performed the experiments: Li Ling, Jiali Zeng, Lanhua Wu, Qianru Zeng, Caijiao Peng, Yubin Huang. They were aware of the group allocation at the different stages of the experiment (during the allocation, the conduct of the experiment, the outcome assessment, and the data analysis). Analyzed the data: Li Ling, Jiali Zeng, Lanhua Wu. Helped perform the analysis with constructive discussions: Li Ling, Jiali Zeng, Lanhua Wu.Drafted the manuscript: Li LingAll authors read and approved the final manuscript.

Funding
This work was supported by the National Natural Science Foundation of China (No. 82304959) and Natural Science Foundation of Chongqing (No. cstc2019jcyj-msxmX0850).

Data availability
All data generated or analysed during this study are included in this published article. The datasets used and/or analysed during the current study are available from the corresponding author on reasonable request.

Declarations

Ethics approval and consent to participate
The research was in compliance with the Helsinki Declaration and approved by the Ethics Committee of the Second Affiliated Hospital of Chongqing Medical University. Written informed consent was obtained from all donors before collecting amnion. Animal experimental protocols were approved by the Ethics Committee of the Second Affiliated Hospital of Chongqing Medical University in March 25, 2020. The approved project was entitled "Effects of Ginsenoside Rg1 combined with human amnion-derived mesenchymal stem cells (hAD-MSCs) on the chemotherapy-induced premature ovarian insufficiency (POI) (permit number 2020-20) ".

Consent for publication
Not applicable.

Competing interests
The authors declare no competing interests.

Author details
[1]The Second Affiliated Hospital of Chongqing Medical University, No. 74, Linjiang Road, Chongqing 400010, China

Received: 22 June 2025 / Accepted: 28 October 2025
Published online: 25 November 2025

References

1. European Society for R, Human POI Embryology Guideline Group on, Webber L, Davies M, Anderson R, Bartlett J, Braat D, Cartwright B, Cifkova R, de Keizer-Schrama S, Hogervorst E, Janse F, Liao L, Vlaisavljevic V, Zillikens C. N. Vermeulen. ESHRE Guideline: management of women with premature ovarian insufficiency. Human Reproduction. 2016;31(5):926 – 37.
2. Hu HQ, Xin XY, Zhu YT, Fan RW, Zhang HL, Ye Y, et al. Application of mesenchymal stem cell therapy for premature ovarian insufficiency: recent advances from mechanisms to therapeutics. World J Stem Cells. 2024;16(1):1–6.
3. Mauri D, Gazouli I, Zarkavelis G, Papadaki A, Mavroeidis L, Gkoura S, Ntellas P, Amylidi AL, Tsali L. Kampletsas. Chemotherapy associated ovarian failure. Front Endocrinol. 2020;11:572388.
4. Ling L, Feng X, Wei T, Wang Y, Wang Y, Zhang W, et al. Effects of low-intensity pulsed ultrasound (LIPUS)-pretreated human amnion-derived mesenchymal stem cell (hAD-MSC) transplantation on primary ovarian insufficiency in rats. Stem Cell Res Ther. 2017;8(1):283.
5. Ling L, Feng X, Wei T, Wang Y, Wang Y, Wang Z, et al. Human amnion-derived mesenchymal stem cell (hAD-MSC) transplantation improves ovarian function in rats with premature ovarian insufficiency (POI) at least partly through a paracrine mechanism. Stem Cell Res Ther. 2019;10(1):46.
6. He F, Yu C, Liu T, Jia H. Ginsenoside Rg1 as an effective regulator of mesenchymal stem cells. Front Pharmacol. 2019;10:1565.
7. Wang S, Zhu R, Li H, Li J, Han Q, Zhao RC. Mesenchymal stem cells and immune disorders: from basic science to clinical transition. Front Med. 2019;13(2):138–51.
8. Phinney DG, Pittenger MF. Concise review: MSC-derived exosomes for cell-free therapy. Stem Cells. 2017;35(4):851–8.
9. Ling L, Wei T, He L, Wang Y, Wang Y, Feng X, et al. Low-intensity pulsed ultrasound activates ERK1/2 and PI3K-Akt signalling pathways and promotes the proliferation of human amnion-derived mesenchymal stem cells. Cell Prolif. 2017. https://doi.org/10.1111/cpr.12383.
10. Parolini O, Alviano F, Bagnara GP, Bilic G, Buhring HJ, Evangelista M, et al. Concise review: isolation and characterization of cells from human term placenta: outcome of the first international workshop on placenta derived stem cells. Stem Cells. 2008;26(2):300–11.
11. Karp JM. Leng Teo. Mesenchymal stem cell homing: the devil is in the details. Cell Stem Cell. 2009;4(3):206–16.
12. Kang SK, Shin IS, Ko MS, Jo JY. Ra. Journey of mesenchymal stem cells for homing: strategies to enhance efficacy and safety of stem cell therapy. Stem Cells Int. 2012;2012:342968.
13. Sadeghi S, Mosaffa N, Huang B, Ramezani F, Tehrani. Protective role of stem cells in POI: current status and mechanism of action, a review Article. Heliyon. 2024;10(1):e23271.
14. Yan L, Wu Y, Li L, Wu J, Zhao F, Gao Z, et al. Clinical analysis of human umbilical cord mesenchymal stem cell allotransplantation in patients with premature ovarian insufficiency. Cell Prolif. 2020;53(12):e12938.
15. Zhang S, Yahaya BH, Pan Y, Liu Y, Lin J. Menstrual blood-derived endometrial stem cell, a unique and promising alternative in the stem cell-based therapy for chemotherapy-induced premature ovarian insufficiency. Stem Cell Res Ther. 2023;14(1):327.
16. Ding L, Yan G, Wang B, Xu L, Gu Y, Ru T, Cui X, Lei L, Liu J, Sheng X, Wang B, Zhang C, Yang Y, Jiang R, Zhou J, Kong N, Lu F, Zhou H, Zhao Y, Chen B, Hu Y, Dai J. Sun. Transplantation of UC-MSCs on collagen scaffold activates follicles in dormant ovaries of POF patients with long history of infertility. Sci China Life Sci. 2018;61(12):1554–65.
17. Feng X, Ling L, Zhang W, Liu X, Wang Y, Luo Y. Xiong. Effects of human Amnion-Derived mesenchymal stem cell (hAD-MSC) transplantation in situ on primary ovarian insufficiency in SD rats. Reproductive Sci. 2020;27(7):1502–12.
18. Shen J, Cao D, Sun JL. Ability of human umbilical cord mesenchymal stem cells to repair chemotherapy-induced premature ovarian failure. World J Stem Cells. 2020;12(4):277–87.
19. Xiao GY, Liu IH, Cheng CC, Chang CC, Lee YH, Cheng WT. Wu. Amniotic fluid stem cells prevent follicle Atresia and rescue fertility of mice with premature ovarian failure induced by chemotherapy. PLoS ONE. 2014;9(9):e106538.
20. Lu G, Li HX, Song ZW, Luo J, Fan YL, Yin YL, et al. Combination of bone marrow mesenchymal stem cells and moxibustion restores cyclophosphamide-induced premature ovarian insufficiency by improving mitochondrial function and regulating mitophagy. Stem Cell Res Ther. 2024;15(1):102.
21. Bahrehbar K, Rezazadeh Valojerdi M, Esfandiari F, Fathi R, Hassani SN, Baharvand H. Human embryonic stem cell-derived mesenchymal stem cells improved premature ovarian failure. World J Stem Cells. 2020;12(8):857–78.
22. Dong J, Zhu G, Wang TC, Shi FS. Ginsenoside Rg1 promotes neural differentiation of mouse adipose-derived stem cells via the miRNA-124 signaling pathway. J Zhejiang Univ Sci B. 2017;18(5):445–8.
23. Guo YH, Zhao S, Du YX, Xing QJ, Chen BL. C. Q. Yu. Effects of ginsenoside Rg1-loaded alginate-chitosan microspheres on human bone marrow stromal cells. Biosci Rep. 2017;37(3):BSR20160566.

24. Gu Y, Zhou J, Wang Q, Fan W, Yin G. Ginsenoside Rg1 promotes osteogenic differentiation of rBMSCs and healing of rat tibial fractures through regulation of GR-dependent BMP-2/SMAD signaling. Sci Rep. 2016;6:25282.
25. Liu Y, Yi L, Wang L, Chen L, Chen X, Wang Y. Ginsenoside Rg1 protects human umbilical cord blood-derived stromal cells against tert-butyl hydroperoxide-induced apoptosis through Akt-FoxO3a-Bim signaling pathway. Mol Cell Biochem. 2016;421(1–2):75–87.
26. Luo Y, Wang B, Liu J, Ma F, Luo D, Zheng Z, et al. Ginsenoside RG1 enhances the paracrine effects of bone marrow-derived mesenchymal stem cells on radiation induced intestinal injury. Aging. 2020;13(1):1132–52.
27. Mohanan P, Subramaniyam S, Mathiyalagan R, Yang DC. Molecular signaling of ginsenosides Rb1, Rg1, and Rg3 and their mode of actions. J Ginseng Res. 2018;42(2):123–32.
28. Ling L, Shu H, Huang Y, Hou J, Hua Y. Effects of ginsenoside Rg1 on the biological behavior of human amnion-derived mesenchymal stem/stromal cells (hAD-MSCs). Stem Cells Int. 2023;2023:7074703.
29. Bao C, Wang Y, Min H, Zhang M, Du X, Han R, et al. Combination of ginsenoside Rg1 and bone marrow mesenchymal stem cell transplantation in the treatment of cerebral ischemia reperfusion injury in rats. Cell Physiol Biochem. 2015;37(3):901–10.
30. Zheng HZ, Fu XK, Shang JL, Lu RX, Ou YF, Chen CL. Ginsenoside Rg1 protects rat bone marrow mesenchymal stem cells against ischemia induced apoptosis through miR-494-3p and ROCK-1. Eur J Pharmacol. 2018;822:154–67.
31. Nishi Y, Yanase T, Mu Y, Oba K, Ichino I, Saito M, Nomura M, Mukasa C, Okabe T, Goto K, Takayanagi R, Kashimura Y, Haji M. Nawata. Establishment and characterization of a steroidogenic human granulosa-like tumor cell line, KGN, that expresses functional follicle-stimulating hormone receptor. Endocrinology. 2001;142(1):437–45.
32. Wang S, Zheng Y, Li J, Yu Y, Zhang W, Song M, Liu Z, Min Z, Hu H, Jing Y, He X, Sun L, Ma L, Esteban CR, Chan P, Qiao J, Zhou Q, Izpisua Belmonte JC, Qu J, Tang F, Liu GH. Single-Cell Transcriptomic Atlas Primate Ovarian Aging Cell. 2020;180(3):585–600. e19.
33. Soncini M, Vertua E, Gibelli L, Zorzi F, Denegri M, Albertini A, Wengler GS. Parolini. Isolation and characterization of mesenchymal cells from human fetal membranes. J Tissue Eng Regen Med. 2007;1(4):296–305.
34. Ko MJ, Lim CY. General considerations for sample size estimation in animal study. Korean J Anesthesiol. 2021;74(1):23–9.
35. Ling L, Hou J, Liu D, Tang D, Zhang Y, Zeng Q, et al. Important role of the SDF-1/CXCR4 axis in the homing of systemically transplanted human amnion-derived mesenchymal stem cells (hAD-MSCs) to ovaries in rats with chemotherapy-induced premature ovarian insufficiency (POI). Stem Cell Res Ther. 2022;13(1):79.
36. Ling L, Hou J, Wang Y, Shu H, Huang Y. Effects of low-intensity pulsed ultrasound on the migration and homing of human amnion-derived mesenchymal stem cells to ovaries in rats with premature ovarian insufficiency. Cell Transplant. 2022;31:9636897221129171.
37. Zhao Y, Ma J, Yi P, Wu J, Zhao F, Tu W, et al. Human umbilical cord mesenchymal stem cells restore the ovarian metabolome and rescue premature ovarian insufficiency in mice. Stem Cell Res Ther. 2020;11(1):466.
38. Chen D, Hu N, Xing S, Yang L, Zhang F, Guo S, et al. Placental mesenchymal stem cells ameliorate NLRP3 inflammasome-induced ovarian insufficiency by modulating macrophage M2 polarization. J Ovarian Res. 2023;16(1):58.
39. Arifin WN. Zahiruddin. Sample size calculation in animal studies using resource equation approach. Malaysian J Med Sci. 2017;24(5):101–5.
40. Rinwa P, Eriksson M, Cotgreave I. Backberg. 3R-Refinement principles: elevating rodent well-being and research quality. Lab Anim Res. 2024;40(1):11.
41. Tang D, Feng X, Ling L, Zhang W, Luo Y, Wang Y, et al. Experimental study for the establishment of a chemotherapy-induced ovarian insufficiency model in rats by using cyclophosphamide combined with busulfan. Regul Toxicol Pharmacol. 2021;122:104915.
42. He L, Ling L, Wei T, Wang Y, Xiong Z. Ginsenoside Rg1 improves fertility and reduces ovarian pathological damages in premature ovarian failure model of mice. Exp Biol Med (Maywood). 2017;242(7):683–91.
43. Dong Z, Xu M, Huang J, Chen L, Xia J, Chen X, et al. The protective effect of ginsenoside Rg1 on aging mouse pancreas damage induced by D-galactose. Exp Ther Med. 2017;14(1):616–22.
44. Byers SL, Wiles MV, Dunn SL. Taft. Mouse estrous cycle identification tool and images. PLoS ONE. 2012;7(4):e35538.
45. Weidner N, Semple JP, Welch WR, Folkman J. Tumor angiogenesis and metastasis–correlation in invasive breast carcinoma. N Engl J Med. 1991;324(1):1–8.
46. Reijnen C, van Weelden WJ, Arts M, Peters JP, Rijken PF, van de Vijver K, Santacana M, Bronsert P, Bulten J, Hirschfeld M, Colas E, Gil-Moreno A, Reques A, Mancebo G, Krakstad C, Trovik J, Haldorsen IS, Huvila J, Koskas M, Weinberger V, Minar L, Jandakova E, Snijders M, van den Berg-van Erp S, Kusters-Vandevelde HVN, Matias-Guiu X, Amant F, consortium E, Massuger L, Bussink J, Pijnenborg JMA. Poor outcome in hypoxic endometrial carcinoma is related to vascular density. Br J Cancer. 2019;120(11):1037–44.
47. Wu Y, Du K, Guan W, Wu D, Tang H, Wang N, Qi J, Gu Z, Yang J. Ding. A novel definition of microvessel density in renal cell carcinoma: angiogenesis plus vasculogenic mimicry. Oncol Lett. 2020;20(5):192.
48. Kim SM, Yoo JY, Hong YH, Lee J, Kim JH. Lee. The effect of growth hormone on ovarian function recovery in a mouse model of ovarian insufficiency. Front Endocrinol. 2023;14:1184977.
49. Sun B, Ma Y, Wang F, Hu L, Sun Y. MiR-644-5p carried by bone mesenchymal stem cell-derived exosomes targets regulation of p53 to inhibit ovarian granulosa cell apoptosis. Stem Cell Res Ther. 2019;10(1):360.
50. Sun L, Li D, Song K, Wei J, Yao S, Li Z, et al. Exosomes derived from human umbilical cord mesenchymal stem cells protect against cisplatin-induced ovarian granulosa cell stress and apoptosis *in vitro*. Sci Rep. 2017;7(1):2552.
51. Huang Y, Zhu M, Liu Z, Hu R, Li F, Song Y, Geng Y, Ma W, Song K. Zhang. Bone marrow mesenchymal stem cells in premature ovarian failure: mechanisms and prospects. Front Immunol. 2022;13:997808.
52. Morgan S, Anderson RA, Gourley C, Wallace WH. N. Spears. How do chemotherapeutic agents damage the ovary? Hum Reprod Update. 2012;18(5):525–35.
53. Li Z, Zhang M, Tian Y, Li Q, Huang X. Mesenchymal stem cells in premature ovarian insufficiency: mechanisms and prospects. Front Cell Dev Biol. 2021;9:718192.
54. Mao J, Smith MF, Rucker EB, Wu GM, McCauley TC, Cantley TC, Prather RS, Didion BA. Day. Effect of epidermal growth factor and insulin-like growth factor I on Porcine preantral follicular growth, antrum formation, and stimulation of granulosal cell proliferation and suppression of apoptosis in vitro. J Anim Sci. 2004;82(7):1967–75.
55. Uzumcu M, Pan Z, Chu Y, Kuhn PE, Zachow R. Immunolocalization of the hepatocyte growth factor (HGF) system in the rat ovary and the anti-apoptotic effect of HGF in rat ovarian granulosa cells *in vitro*. Reproduction. 2006;132(2):291–9.
56. Westfall SD, Hendry IR, Obholz KL, Rueda BR. Davis. Putative role of the phosphatidylinositol 3-kinase-Akt signaling pathway in the survival of granulosa cells. Endocrine. 2000;12(3):315–21.
57. Yu YS, Sui HS, Han ZB, Li W, Luo MJ. Tan. Apoptosis in granulosa cells during follicular atresia: relationship with steroids and insulin-like growth factors. Cell Res. 2004;14(4):341–6.
58. Takahashi A, Yousif A, Hong L, Chefetz I. Premature ovarian insufficiency: pathogenesis and therapeutic potential of mesenchymal stem cell. J Mol Med. 2021;99(5):637–50.
59. Leverrier Y, Thomas J, Mathieu AL, Low W, Blanquier B. Marvel. Role of PI3-kinase in Bcl-X induction and apoptosis Inhibition mediated by IL-3 or IGF-1 in Baf-3 cells. Cell Death Differ. 1999;6(3):290–6.
60. Cardone MH, Roy N, Stennicke HR, Salvesen GS, Franke TF, Stanbridge E, Frisch S. Reed. Regulation of cell death protease caspase-9 by phosphorylation. Science. 1998;282(5392):1318–21.
61. Chen H, Liu C, Zhu S, Li S, Zhang Q, Song L, et al. The therapeutic effect of stem cells on chemotherapy-induced premature ovarian failure. Curr Mol Med. 2021;21(5):376–84.
62. Celik O, Ak M, Sahin E, Senturk S, Ugur K, Celik S, Celik N, Cengiz F, Muderris II, Capar M, Sahin I. S. Aydin. Intra-ovarian stem cell transplantation in management of premature ovarian insufficiency: towards the induced Oogonial Stem Cell (iOSC). Cellular and Molecular Biology (Noisy-Le-Grand, France). 2020;66(1):114 – 21.
63. Bedoschi G, Navarro PA, Oktay K. Chemotherapy-induced damage to ovary: mechanisms and clinical impact. Future Oncol. 2016;12(20):2333–44.
64. Cai X, Fu H, Wang Y, Liu Q, Wang X. Depletion of GPSM1 enhances ovarian granulosa cell apoptosis via cAMP-PKA-CREB pathway in vitro. J Ovarian Res. 2020;13(1):136.
65. Liang M, Zhou J, Sun X, He C, Zhang K, Hu K. Effects of bisphenol A on apoptosis of ovarian preantral follicular granulosa cells and ovarian development in mice. Nan Fang Yi Ke Da Xue Xue Bao J South Med Univ. 2021;41(1):93–9.
66. Bao R, Xu P, Wang Y, Wang J, Xiao L, Li G, et al. Bone marrow derived mesenchymal stem cells transplantation rescues premature ovarian insufficiency induced by chemotherapy. Gynecol Endocrinol. 2018;34(4):320–6.
67. Zhang H, Luo Q, Lu X, Yin N, Zhou D, Zhang L, Zhao W, Wang D, Du P, Hou Y, Zhang Y. Yuan. Effects of hPMSCs on granulosa cell apoptosis and AMH

expression and their role in the restoration of ovary function in premature ovarian failure mice. Stem Cell Res Ther. 2018;9(1):20.
68. Shi YQ, Zhu XT, Zhang SN, Ma YF, Han YH, Jiang Y, et al. Premature ovarian insufficiency: a review on the role of oxidative stress and the application of antioxidants. Front Endocrinol. 2023;14:1172481.
69. Sai T, Goto Y, Yoshioka R, Maeda A, Matsuda F, Sugimoto M, Wongpanit K, Jin HZ, Li JY. Manabe. Bid and Bax are involved in granulosa cell apoptosis during follicular Atresia in Porcine ovaries. J Reprod Dev. 2011;57(3):421–7.
70. Huang Q, Liu B, Jiang R, Liao S, Wei Z, Bi Y, et al. G-CSF-mobilized peripheral blood mononuclear cells combined with platelet-rich plasma accelerate restoration of ovarian function in cyclophosphamide-induced POI ratsdagger. Biol Reprod. 2019;101(1):91–101.
71. Wang L, Li M, Liu J, Nie G, Li Y, Yang H. Protective effect of Huyang Yangkun formula on ovarian function in premature ovarian insufficiency rats based on apoptotic mechanism. J Ethnopharmacol. 2021;280:114477.
72. Raei Sadigh A, Darabi M, Salmassi A, Hamdi K, Farzadi L, Ghasemzadeh A, et al. Fractalkine and apoptotic/anti-apoptotic markers in granulosa cells of women with polycystic ovarian syndrome. Mol Biol Rep. 2020;47(5):3593–603.
73. Xu H, Xia Y, Qin J, Xu J, Li C, Wang Y. Effects of low intensity pulsed ultrasound on expression of B-cell lymphoma-2 and BCL2-associated X in premature ovarian failure mice induced by 4-vinylcyclohexene diepoxide. Reprod Biol Endocrinol. 2021;19(1):113.
74. Fu X, He Y, Xie C, Liu W. Bone marrow mesenchymal stem cell transplantation improves ovarian function and structure in rats with chemotherapy-induced ovarian damage. Cytotherapy. 2008;10(4):353–63.
75. Huang B, Qian C, Ding C, Meng Q, Zou Q, Li H. Fetal liver mesenchymal stem cells restore ovarian function in premature ovarian insufficiency by targeting MT1. Stem Cell Res Ther. 2019;10(1):362.
76. Deng T, He J, Yao Q, Wu L, Xue L, Wu M, et al. Human umbilical cord mesenchymal stem cells improve ovarian function in chemotherapy-induced premature ovarian failure mice through inhibiting apoptosis and inflammation via a paracrine mechanism. Reprod Sci. 2021;28(6):1718–32.
77. Elfayomy AK, Almasry SM, El-Tarhouny SA, Eldomiaty MA. Human umbilical cord blood-mesenchymal stem cells transplantation renovates the ovarian surface epithelium in a rat model of premature ovarian failure: possible direct and indirect effects. Tissue Cell. 2016;48(4):370–82.
78. Zhang Y, Xia X, Yan J, Yan L, Lu C, Zhu X, et al. Mesenchymal stem cell-derived angiogenin promotes primodial follicle survival and angiogenesis in transplanted human ovarian tissue. Reprod Biol Endocrinol. 2017;15(1):18.
79. Ding C, Zou Q, Wang F, Wu H, Chen R, Lv J, et al. Human amniotic mesenchymal stem cells improve ovarian function in natural aging through secreting hepatocyte growth factor and epidermal growth factor. Stem Cell Res Ther. 2018;9(1):55.
80. Hu CL, Cowan RG, Harman RM, Quirk SM. Cell cycle progression and activation of Akt kinase are required for insulin-like growth factor I-mediated suppression of apoptosis in granulosa cells. Mol Endocrinol. 2004;18(2):326–38.
81. Quirk SM, Harman RM, Cowan RG. Regulation of Fas antigen (Fas, CD95)-mediated apoptosis of bovine granulosa cells by serum and growth factors. Biol Reprod. 2000;63(5):1278–84.
82. Sameni HR, Seiri M, Safari M, Tabrizi Amjad MH, Khanmohammadi N. Zarbakhsh. Bone marrow stromal cells with the granulocyte Colony-Stimulating factor in the management of Chemotherapy-Induced ovarian failure in a rat model. Iran J Med Sci. 2019;44(2):135–45.
83. Bencomo E, Perez R, Arteaga MF, Acosta E, Pena O, Lopez L, et al. Apoptosis of cultured granulosa-lutein cells is reduced by insulin-like growth factor I and may correlate with embryo fragmentation and pregnancy rate. Fertil Steril. 2006;85(2):474–80.
84. Yu Y, Li W, Han Z, Luo M, Chang Z, Tan J. The effect of follicle-stimulating hormone on follicular development, granulosa cell apoptosis and steroidogenesis and its mediation by insulin-like growth factor-I in the goat ovary. Theriogenology. 2003;60(9):1691–704.
85. Baker J, Hardy MP, Zhou J, Bondy C, Lupu F, Bellve AR. A. Efstratiadis. Effects of an Igf1 gene null mutation on mouse reproduction. Mol Endocrinol. 1996;10(7):903–18.
86. Gabr H, Rateb MA, El Sissy MH, Ahmed Seddiek H. Ali Abdelhameed Gouda. The effect of bone marrow-derived mesenchymal stem cells on chemotherapy induced ovarian failure in albino rats. Microsc Res Tech. 2016;79(10):938–47.
87. Kulik G, Klippel A, Weber MJ. Antiapoptotic signalling by the insulin-like growth factor I receptor, phosphatidylinositol 3-kinase, and Akt. Mol Cell Biol. 1997;17(3):1595–606.
88. Datta SR, Dudek H, Tao X, Masters S, Fu H, Gotoh Y, et al. Akt phosphorylation of BAD couples survival signals to the cell-intrinsic death machinery. Cell. 1997;91(2):231–41.
89. Lin S, Zhang Q, Shao X, Zhang T, Xue C, Shi S, Zhao D, Lin Y. IGF-1 promotes angiogenesis in endothelial cells/adipose-derived stem cells co-culture system with activation of PI3K/Akt signal pathway. Cell Proliferation. 2017;50(6):e12390.
90. Johnson AL, Bridgham JT, Swenson JA. Activation of the Akt/protein kinase B signaling pathway is associated with granulosa cell survival. Biol Reprod. 2001;64(5):1566–74.
91. John GB, Shidler MJ, Besmer P. Castrillon. Kit signaling via PI3K promotes ovarian follicle maturation but is dispensable for primordial follicle activation. Dev Biol. 2009;331(2):292–9.
92. Zhong K, Huang Y, Chen R, Pan Q, Li J, Xi X. The protective effect of ginsenoside Rg1 against sepsis-induced lung injury through PI3K-Akt pathway: insights from molecular dynamics simulation and experimental validation. Sci Rep. 2024;14(1):16071.
93. Hu J, Gu Y, Fan W. Rg1 protects rat bone marrow stem cells against hydrogen peroxide-induced cell apoptosis through the PI3K/Akt pathway. Mol Med Rep. 2016;14(1):406–12.
94. Liu S, Pei H, Chen W, Zhu X, Wang Y, Li J, et al. Evaluating the effect of ginsenoside Rg1 on CPF-induced brain injury in mice via PI3k/AKT pathway. J Biochem Mol Toxicol. 2023;37(5):e23319.
95. Cao H, Wei W, Xu R, Cui X. Ginsenoside Rg1 can restore hematopoietic function by inhibiting Bax translocation-mediated mitochondrial apoptosis in aplastic anemia. Sci Rep. 2021;11(1):12742.
96. Xu Z, Li X, Shen G, Zou Y, Zhang H, Yang K, et al. The protective effect of ginsenoside Rg1 on apoptosis in human ankle joint traumatic arthritis chondrocytes. Evidence-Based Complementary and Alternative Medicine. 2022;2022:6798377.
97. Park HS, Chugh RM, Elsharoud A, Ulin M, Esfandyari S, Aboalsoud A, et al. Safety of intraovarian injection of human mesenchymal stem cells in a premature ovarian insufficiency mouse model. Cell Transplant. 2021;30:963689720988502.
98. Wang Z, Wang L, Jiang R, Li C, Chen X, Xiao H, et al. Ginsenoside Rg1 prevents bone marrow mesenchymal stem cell senescence via NRF2 and PI3K/Akt signaling. Free Radic Biol Med. 2021;174:182–94.

Publisher's Note

Springer Nature remains neutral with regard to jurisdictional claims in published maps and institutional affiliations.